Title
SEPARABLE POTENTIAL MODELS OF THE NUCLEON-NUCLEON INTERACTION

Author
Mongan, Thomas R.

Publication Date
1968-10-03

UCRL-18501

Cy.2

University of California

Ernest O. Lawrence Radiation Laboratory

SEPARABLE POTENTIAL MODELS OF THE NUCLEON-NUCLEON INTERACTION

Thomas R. Mongan

October 3, 1968

T/P

UCRL-18501
Cy.2

DISCLAIMER

Submitted to Physical Review

UCRL-18501
Preprint

UNIVERSITY OF CALIFORNIA

Lawrence Radiation Laboratory
Berkeley, California

AEC Contract No. W-7405-eng-48

SEPARABLE POTENTIAL MODELS OF THE NUCLEON-NUCLEON INTERACTION

Thomas R. Mongan

October 3, 1968

SEPARABLE POTENTIAL MODELS OF THE NUCLEON-NUCLEON INTERACTION*

Thomas R. Mongan

Lawrence Radiation Laboratory
University of California
Berkeley, California

October 3, 1968

ABSTRACT

We present four different separable potential models of the nucleon-nucleon interaction which fit both the low-energy data and the MacGregor-Arndt-Wright phase parameters for partial waves through $J = 4$ in the energy range 0 to 400 MeV. The partial-wave scattering amplitudes resulting from our potentials have driving singularities at real negative values of the complex energy variable, and the appropriate amplitudes contain the deuteron pole and the singlet antibound state pole at the correct energies. The present work extends and completes the results of an earlier paper.

INTRODUCTION

Previously,[1] we gave three separable potentials which fit the nucleon-nucleon scattering data. Now the Livermore group of MacGregor, Arndt, and Wright[2] has published the last of a series of papers on the determination of the nucleon-nucleon phase parameters. The appearance of these data has prompted us to extend and complete the work of Ref. 1.

We shall set forth four different separable potential models of the nucleon-nucleon interaction. When separable potentials are inserted in the Lippmann-Schwinger integral equation for the off-energy-shell two-nucleon partial-wave scattering amplitude, the kernel of the equation becomes separable. Consequently the Lippmann-Schwinger equation can be solved algebraically. The resulting off-shell partial-wave amplitude is separable in the incident and outgoing relative momentum variables. Also, the off-shell amplitude is guaranteed to satisfy the five general nondynamical requirements laid down in Ref. 1, if the separable potential form factors are properly chosen. That is, the off-shell partial-wave amplitudes resulting from our separable potential models:

(i) Reduce to the correct on-shell amplitudes.

(ii) Satisfy off-energy-shell two-particle unitarity.

(iii) Have reasonable analyticity properties.

(iv) Are time-reversal invariant.

(v) Have the proper threshold behavior in both energy and momentum variables.

Because of their extreme simplicity, these separable potential models should be useful in multiparticle scattering calculations. The

fact that the off-shell behavior of these models is determined by the choice of the separable potential form factors and the resulting amplitudes can be written as an off-shell factor multiplying the on-shell amplitude makes them useful in probing the off-shell behavior of two-body scattering amplitudes.

BASIC EQUATIONS

We consider models of the nucleon-nucleon interaction with a separable potential of the form

$$V_{\ell\ell'}(p,p') = [i^{(\ell'-\ell)}]\cdot[g_\ell(p)\, g_{\ell'}(p') - h_\ell(p)\, h_{\ell'}(p')] \quad . \quad (1)$$

This potential is to be inserted into the nonrelativistic two-particle partial-wave Lippmann-Schwinger equation, which for uncoupled waves is

$$T_\ell(p,p';\, k^2) = V_\ell(p,p') + \frac{2\mu}{\hbar^2} \int_0^\infty \frac{dq\, q^2\, V_\ell(p,q)\, T_\ell(q,p';\, k^2)}{k^2 - q^2 + i\epsilon} \,, \quad (2)$$

where the c.m. kinetic energy $E = \hbar^2 k^2/2\mu$, and μ is the reduced mass of the two nucleons. For coupled waves, the Lippmann-Schwinger equation is

$$T_{\ell\ell'}(p,p';\, k^2) = V_{\ell\ell'}(p,p') + \frac{2\mu}{\hbar^2} \sum_{j=J-1}^{J+1} \int_0^\infty \frac{dq\, q^2\, V_{\ell j}(p,q)\, T_{j\ell'}(q,p';\, k^2)}{k^2 - q^2 + i\epsilon} \,.$$

The partial-wave T matrix obtained from the Lippmann-Schwinger equation is related to the partial-wave S matrix by

$$S_{\ell\ell'}(k^2) = 1 - 2\pi i\, \rho_E\, T_{\ell\ell'}(k^2) \,,$$

where $\rho_E = \mu k/\hbar^2$. For uncoupled waves, the S matrix is given in terms of the phase shifts by $S_\ell(k^2) = e^{2i\delta_\ell(k^2)}$ or

$S_\ell(k^2) = 1 + 2i\, e^{i\delta_\ell(k^2)} \sin \delta_\ell(k^2)$, whence

$\tan 2\delta_\ell(k^2) = \dfrac{-2\pi\, \rho_E\, \mathrm{Re}\, T_\ell(k^2)}{1 + 2\pi\, \rho_E\, \mathrm{Im}\, T_\ell(k^2)}$. Alternatively, the T matrix can be expressed in terms of the phase shifts as

$$T_\ell(k^2) = -\frac{1}{\pi\rho_E}\, e^{i\delta_\ell(k^2)} \sin \delta_\ell(k^2) \ ,$$

whence $\tan \delta_\ell(k^2) = \mathrm{Im}\, T_\ell(k^2)/\mathrm{Re}\, T_\ell(k^2)$. For coupled waves, we use the Stapp[3] parameterization of the S matrix

$$S = \begin{pmatrix} \cos 2\epsilon\, e^{2i\delta_{J-1}} & i \sin 2\epsilon\, e^{i(\delta_{J-1}+\delta_{J+1})} \\ i \sin 2\epsilon\, e^{i(\delta_{J-1}+\delta_{J+1})} & \cos 2\epsilon\, e^{2i\delta_{J+1}} \end{pmatrix}$$

Then, the coupled wave phase shifts and mixing parameters are given in terms of the T-matrix elements by

$$\tan 2\delta_{J-1} = \frac{-2\pi\, \rho_E\, \mathrm{Re}\, T_{J-1,J-1}(k^2)}{1 + 2\pi\rho_E\, \mathrm{Im}\, T_{J-1,J-1}(k^2)} \ ,$$

$$\tan 2\delta_{J+1} = \frac{-2\pi\, \rho_E\, \mathrm{Re}\, T_{J+1,J+1}(k^2)}{1 + 2\pi\, \rho_E\, \mathrm{Im}\, T_{J+1,J+1}(k^2)} \ ,$$

$$\sin 2\epsilon = \frac{-2\pi\, \rho_E\, \mathrm{Re}\, T_{OD}(k^2)}{\cos(\delta_{J+1} + \delta_{J-1})} \ ,$$

where $T_{OD}(k^2) = T_{J-1,J+1}(k^2) = T_{J+1,J-1}(k^2)$.

The separable potential formalism allows us to solve explicitly for the T matrix in the form $T_{\ell\ell'}(p,p';k^2) = N_{\ell\ell'}(p,p';k^2)/D_J(k^2)$, as well as the deuteron wave function, the deuteron D state probability, and the deuteron quadrupole moment, in terms of the separable potential form factors and certain integrals over these form factors. These results can be found in Ref. 1.

For $J = 1$, the triplet scattering length a_t, the triplet effective range r_t and the deuteron binding energy are related by

$$r_t = \frac{2}{k_D}\left(1 - \frac{1}{a_t k_D}\right) , \tag{3}$$

where the deuteron binding energy is $E_D = \hbar^2 k_D^2/2\mu$. The position of the singlet antibound state pole in the $^1S_0$ partial wave is related to the singlet effective range a_s and the singlet scattering length r_s by

$$k_V = [1 - [1 - (2r_s/a_s)]^{\frac{1}{2}}]/r_s , \tag{4}$$

where the pole occurs at the negative energy $E_V = -\hbar^2 k_V^2/2\mu$ on the second or unphysical sheet of the complex energy Riemann surface. The scattering lengths are given by $a_s = \lim_{k\to 0} \frac{\pi\mu}{\hbar^2} \operatorname{Re} T_0(k^2)$ and $a_t = \lim_{k\to 0} \frac{\pi\mu}{\hbar} \operatorname{Re} T_{00}(k^2)$, where $T_0(k^2)$ is the transition amplitude for $^1S_0$ scattering and $T_{00}(k^2)$ is the transition matrix element for $J = 1$, $\ell = \ell' = 0$.

We take for the nucleon mass M the average of the neutron and proton masses, so $2\mu c^2 = Mc^2 = 938.903$ MeV and $\hbar c = 197.32$ MeV F. We take the deuteron binding energy $E_D = 2.22452$ MeV and the triplet scattering length $a_t = 5.396$ F, which yields a triplet effective range $r_t = 1.726$ F. We set the singlet antibound state at an energy $E_V = -0.0665$ MeV on the second sheet of the complex energy Riemann surface and we take the singlet scattering length $a_s = -23.678$ F, which yields a singlet effective range $r_s = 2.729$ F.

FORM FACTORS

The choice of a functional form for the repulsive form factor $g_\ell(p)$ and the attractive form factor $h_\ell(p)$ in Eq. (1) determines the off-shell behavior, the threshold behavior, and the analyticity properties of the off-shell scattering amplitudes as well as the asymptotic properties of the phase parameters. We have been particularly careful to choose functional forms which lead to an on-shell scattering amplitude with driving singularities which lie only on the real negative axis in the complex energy plane. Thus our amplitudes have a singularity structure similar to that obtained from the fully relativistic theory of the nucleon-nucleon partial-wave amplitudes.

In Case I, the form factors have the functional form $p^\ell/(p^2 + a^2)^{(\ell+1)/2}$, which has an asymptotic behavior like $1/p$ as $p \to \infty$, whereas in Case II, the form factors are of the form $p^\ell/(p^2 + a^2)^{(\ell+2)/2}$, which goes as $1/p^2$ as $p \to \infty$. These cases correspond to choosing the first two members of the family of form factor shapes discussed in Ref. 1. Of course, all our choices of separable potential form factors behave like p^ℓ at threshold, in order to produce the proper behavior of the phase parameters at threshold. Case I and II in this paper differ from the corresponding cases in Ref. 1 in that we do not introduce any specially modified repulsive form factors.

For Case III, we take form factors like

$$\left[\frac{1}{p^2} Q_\ell\left(1 + \frac{\mu^2}{2p^2}\right)\right]^{\frac{1}{2}}$$

except in the partial waves $^1S_0$, $^3P_0$, $^3S_1$, and $^1P_1$, where the repulsive form factors have the form

$$\frac{p^2}{\left(p^2 + \frac{\mu^2}{4}\right)}\left[\frac{1}{p^2} Q_\ell\left(1 + \frac{\mu^2}{2p^2}\right)\right]^{\frac{1}{2}} .$$

The Q_ℓ functions are Legendre functions of the second kind. Both these forms have an asymptotic behavior like $[(\ell n\ p^2)/p^2]^{\frac{1}{2}}$ as $p \to \infty$, and lead to on-shell amplitudes with cut singularities on the negative real energy axis. Separable potential form factors like those used in Case III were first introduced by Mitra[4] and we have used them because they promise the most realistic analyticity structure. This promise is belied by the fact that we must introduce special repulsive form factors, which have a pole at the start of the repulsive cut, in order to fit the phase shifts in the partial waves $^1S_0$, $^3P_0$, $^3S_1$, and $^1P_1$. In fact, the Case III fits are the least successful of our fits.

Finally, in Case IV, we choose form factors of the form $p^\ell/(p^2 + a^2)^{(\ell+1)}$, which behave as $1/p^{\ell+2}$ as $p \to \infty$. These form factors were chosen because they lead to off-shell amplitudes with the same asymptotic behavior in the momentum variables as the off-shell amplitude arising from a superposition of Yukawa potentials. This is easily seen by noting that a Yukawa potential in momentum space has the form $V_\ell(p,q) \sim \frac{1}{pq} Q_\ell\left(\frac{p^2 + q^2 + \mu^2}{2pq}\right)$, and the insertion of this potential into the Lippman-Schwinger equation (1) leads to an off-shell amplitude $t_\ell(p,q; k^2)$, which behaves like $1/p^{\ell+2}$ as $p \to \infty$ and like $1/q^{\ell+2}$ as $q \to \infty$.

In the $\ell = 0$ partial wave, the Case II and Case IV form factors are identical. Case IV has the added advantage that all the integrals arising in the separable potential formalism can, in principle, be done in closed form.

FIT TO THE NUCLEON-NUCLEON DATA

We have fitted our potentials to the MacGregor-Arndt-Wright (Livermore) nucleon-nucleon phase parameters for laboratory kinetic energy from 0 to 400 MeV for the partial waves through $J = 4$. For each phase parameter we used the 28 data points, in the range 0 to 400 MeV laboratory kinetic energy E, provided by the energy-dependent phase parameter determination of MacGregor, Arndt, and Wright.

The fitting was accomplished on a CDC-6600 electronic computer at Lawrence Radiation Laboratory using LSQMIN, a least squares minimization program developed by Eric Beals. The program LSQMIN searches for the values of the potential parameters that minimize the sum of the squares of the residuals at the 28 data points,

$$\sum R^2 = \sum_{i=1}^{28} [\delta_\ell^{expt}(E_i) - \delta_\ell^{fit}(E_i)]^2 ,$$

for uncoupled waves, and

$$\sum R^2 = \sum_{i=1}^{28} [\delta_{J-1}^{expt}(E_i) - \delta_{J-1}^{fit}(E_i)]^2 + \sum_{i=1}^{28} [\epsilon_J^{expt}(E_i) - \epsilon_J^{fit}(E_i)]^2 + \sum_{i=1}^{28} [\delta_{J+1}^{expt}(E_i) - \delta_{J+1}^{fit}(E_i)]^2 ,$$

for coupled waves.

The potential parameters that yield the best fit to the phase parameters are given in Tables I to VIII, where we have included the

values of $\sum R^2$, since a comparison of these numbers for a single partial-wave or coupled-wave system gives an indication of the relative goodness of fit of the four cases.

We have displayed our fits to the phase parameters graphically in Figs. 1 through 22, where the curve marked Δ at 100 MeV intervals is the data value of the phase parameter in degrees and is read with the left-hand scale. The other curves are the absolute error (fitted value minus data value) in degrees of the various fits, and are read with the right-hand scale. The dashed curve represents the Case I fit, the solid curve marks the Case II fit, the dotted curve indicates the Case III fit, and the dot-dash curve denotes the Case IV fit.

For the convenience of those who would like to use these fits neglecting partial waves with $\ell > \ell_{max}$, where ℓ_{max} is 0, 1, 2 or 3, we have fitted the coupled waves $^3S_1$, $^3P_2$, $^3D_3$, and $^3F_4$, assuming $\epsilon_J = 0$ and neglecting δ_{J+1} in each case. These results are presented in Tables IX through XII and Figs. 23 through 26.

We present the low-energy and bound-state parameters resulting from our potential models in Table XIII. In Table XIV we give the maximum positive and negative values of the errors and the energies at which they occur, for each fitting case in each partial wave. Similarly, Table XV lists the maximum error excursions for the partial waves $^3S_1$, $^3P_2$, $^3D_3$, and $^3F_4$ treated as uncoupled waves. Table XVI gives the grand total of the sum of the squares of the residuals in each fitting case. To form this sum, we sum the squares of the residuals

in each uncoupled partial wave and each coupled wave system through $J = 4$. The results show that Case II gives the best overall fit to the nucleon-nucleon scattering data.

In the partial wave $^1S_0$ we fit the phase shift and the three low-energy parameters: scattering length, virtual (antibound) state pole position, and effective range. These three parameters are related by Eq. (4), so only two of them are independent. Consequently, we choose the scattering length $a_s = -23.678$ F and set the antibound state pole at $E_V = -0.0665$ MeV on the second sheet of the complex energy Riemann surface, which implies a singlet effective range $r_s = 2.729$ F. The antibound state pole on the second or unphysical sheet leads to a zero in the S matrix at the same energy on the physical sheet of the complex energy surface. In addition, the zero of the $^1S_0$ phase shift at 249.5 MeV implies that the N function in the separable potential formula for the on-shell T matrix, $T_\ell(k^2) = N_\ell(k^2)/D_\ell(k^2)$, is zero at 249.5 MeV. To fit the $^1S_0$ partial wave, we use the conditions that the S matrix be zero at $E_V = -0.0665$ MeV and that the N function be zero at 249.5 MeV to determine the attractive and repulsive coupling strengths, and search for the values of the attractive and repulsive inverse ranges which give the best fit to the phase shift and scattering length. We then used Eq. (4) to determine the value of the effective range produced by the separable potential models. Our $^1S_0$ scattering amplitudes are, therefore, guaranteed to contain the singlet antibound state pole at the correct position on the unphysical sheet.

In the construction of our separable potential models, we have made the tacit assumption of charge independence. When fitting the $^1S_0$ phase shifts, we biased the search procedure to insure the correct values of a_s and r_s. However, the MacGregor-Arndt-Wright $^1S_0$ phase shifts are fitted to the proton-proton scattering length and effective range at low energy, and this explains the discrepancy between our fits and the phase shift data at low energies. We can fit the $^1S_0$ phase shifts quite closely, but then the absolute value of the scattering length becomes smaller. Note that the greatest error in our fits to the $^1S_0$ phase shift occurs at 400 MeV, where the data value of the phase shift is $-23.27°$. However, the energy-independent determination of MacGregor, Arndt, and Wright gives a $^1S_0$ phase shift of $-19.35°$ at 425 MeV, so our fits deviate from the energy dependent data in the direction of the energy-independent value. In the absence of a charge dependent determination of the $^1S_0$ phase shifts, we have presented what we feel is the best compromise.

When we fit the $^3P_0$ phase, which has a zero at 204 MeV, we use the condition that the N function of the on-shell T matrix is zero at 204 MeV to determine the repulsive coupling strength. We then search for the values of the attractive coupling strength and the attractive and repulsive inverse ranges which produce the best fit to the phase shift data. However, in Case III, we had to search with all four parameters free to obtain a reasonable fit.

If we consider the partial wave $^3S_1$ as if it were uncoupled, we wish the S matrix, and thus the T matrix, to have the deuteron pole

at $E_D = -2.22452$ MeV on the physical sheet. This is accomplished by determining the attractive coupling strength from the condition that the D function in the separable potential expression for the on-shell T matrix have a zero at the deuteron pole position. Then we search for the values of the repulsive coupling strength and the attractive and repulsive inverse ranges which yield the best fit to the phase shift and scattering length, obtaining the effective range from Eq. (3).

When we consider the coupled waves with $J = 1$, we again guarantee the correct binding energy for the deuteron by obtaining the attractive strength in $\ell = 0$ from the condition that $D_{J=1}(k^2) = 0$ at $E_D = -2.22452$. Next we search for the values of the remaining seven potential parameters which give the best fit to the phase shifts, mixing parameter, scattering length, deuteron quadrupole moment, and D-state probability. We obtain the effective range from Eq. (3). Since the quadrupole moment of the deuteron is sensitive to the off-energy-shell behavior of the nucleon-nucleon interaction, we weight this quantity so that our searching routines are heavily biased in favor of those parameter sets which lead to a nearly correct quadrupole moment. We find that the resulting D-state probabilities are quite low, but since the available estimates of the D-state probability are imprecise and somewhat model dependent, we do not feel that this is a serious drawback.

As an independent check on our work, our separable potential models were put into computer programs which solve the Lippmann-Schwinger Eqs. (1) and (2), with arbitrary well-behaved potentials,

as complex matrix inversion problems. The latter programs were developed completely independently of the present work, and the agreement of the T matrices and phase parameters calculated from the two approaches constitutes the desired check of our work.

In conclusion, we suggest that whenever possible the form $T_{\ell\ell'}(p,p';\, k^2) = F_{\ell\ell'}(p,p';k^2)\, T_{\ell\ell'}(k^2)$ be used in calculations when $k^2 > 0$, with $F_{\ell\ell'}(p,p';\, k^2)$ obtained from the separable potential models and $T_{\ell\ell'}(k^2)$ expressed directly in terms of the experimental phase parameters. This separation has been discussed in Ref. 1, and it guarantees that the effect of on-shell two-body scattering is taken into account as accurately as possible in any calculation involving off-energy-shell two-body partial-wave scattering amplitudes, while retaining the advantage of separability in incident and outgoing momentum variables.

FOOTNOTES AND REFERENCES

* This work was supported in part by the U.S. Atomic Energy Commission.

1. T. R. Mongan, Phys. Rev., to be published. We shall call this Ref. 1.

2. M. H. MacGregor, R. A. Arndt, and R. M. Wright, Phys. Rev. 169, 1128 (1968); M. H. MacGregor, R. A. Arndt, and R. M. Wright, to be published.

3. H. P. Stapp, T. J. Ypsilantis, and N. Metropolis, Phys. Rev. 105, 302 (1957).

4. A. N. Mitra, Phys. Rev. 123, 1892 (1961).

Table I. Case I fits to nucleon-nucleon phase shifts in uncoupled partial waves. These partial waves are fitted by the separable potential

$$V_\ell(p, p') = g_\ell(p)\, g_\ell(p') - h_\ell(p)\, h_\ell(p') \quad ,$$

where the form factors are

$$g_\ell(p) = C_R p^\ell/(p^2 + a_R^2)^{(\ell+1)/2} \qquad h_\ell(p) = C_A p^\ell/(p^2 + a_A^2)^{(\ell+1)/2} \quad .$$

The units of the attractive inverse range a_A and the repulsive inverse range a_R are inverse fermis (F^{-1}, $1F = 10^{-13}$ cm). The units of the attractive coupling strength C_A and the repulsive coupling strength C_R are $(\text{MeV F})^{\frac{1}{2}}$. Dashes indicate that a form factor is to be set equal to zero. ΣR^2 is the sum of the squares of the residuals

$$\Sigma R^2 \equiv \sum_{i=1}^{28} [\delta_\ell{}^{\text{expt}}(E_i) - \delta_\ell{}^{\text{fit}}(E_i)]^2$$

at the 28 data points in the range 0 to 400 MeV.

Table I (Continued).

Partial wave	Repulsive potential parameters $a_R(F^{-1})$	$C_R(\text{MeV F})^{\frac{1}{2}}$	Attractive potential parameters $a_A(F^{-1})$	$C_A(\text{MeV F})^{\frac{1}{2}}$	ΣR^2
Singlet					
$^1S_0$	2.331	52.45	1.855	41.36	469.3
$^1P_1$	1.138	49.83	1.103	46.16	73.93
$^1D_2$	-	-	1.418	4.817	5.253
$^1F_3$	1.059	4.118	-	-	4.885
$^1G_4$	-	-	1.076	2.300	0.139
Triplet					
$^3P_0$	2.258	118.2	1.326	16.48	18.04
$^3P_1$	0.697	3.498	2.322	18.89	0.091
$^3D_2$	-	-	0.992	5.482	15.95
$^3F_3$	0.837	2.347	-	-	0.120
$^3G_4$	-	-	0.970	3.851	1.476

Table II. Case II fits to nucleon-nucleon phase shifts in uncoupled partial waves. These partial waves are fitted by the separable potential

$$V_\ell(p,p') = g_\ell(p)\, g_\ell(p') - h_\ell(p)\, h_\ell(p') \quad ,$$

where the form factors are

$$g_\ell(p) = C_R p^\ell/(p^2 + a_R^2)^{(\ell+2)/2} \qquad h_\ell(p) = C_A p^\ell/(p^2 + a_A^2)^{(\ell+2)/a} \quad .$$

The units of the attractive inverse range a_A and the repulsive inverse range a_R are inverse fermis (F^{-1}, $1F = 10^{-13}$ cm). The units of the attractive coupling strength C_A and the repulsive coupling strength C_R are $(MeV/F)^{\frac{1}{2}}$. Dashes indicate that a form factor is to be set equal to zero. ΣR^2 is the sum of the squares of the residuals

$$\Sigma R^2 = \sum_{i=1}^{28} [\delta_\ell{}^{expt}(E_i) - \delta_\ell{}^{fit}(E_i)]^2 \quad ,$$

at the 28 data points in the range 0 to 400 MeV.

Table II (Continued).

Partial wave	Repulsive potential parameters $a_R(F^{-1})$	Repulsive potential parameters $C_R(MeV/F)^{\frac{1}{2}}$	Attractive potential parameters $a_A(F^{-1})$	Attractive potential parameters $C_R(MeV/F)^{\frac{1}{2}}$	R^2
Singlet					
$^1S_0$	6.157	302.0	1.786	27.33	456.3
$^1P_1$	1.410	40.88	1.258	30.21	43.52
$^1D_2$	-	-	1.944	21.09	8.577
$^1F_3$	1.470	14.16	-	-	7.514
$^1G_4$	-	-	1.425	8.502	0.257
Triplet					
$^3P_0$	4.460	988.1	1.313	13.94	11.34
$^3P_1$	2.178	45.63	-	-	56.06
$^3D_2$	-	-	1.468	20.60	44.31
$^3F_3$	1.213	7.247	-	-	0.766
$^3G_4$	-	-	1.317	14.04	3.894

Table III. Case III fits to nucleon-nucleon phase shifts in uncoupled partial waves. These partial waves are fitted by the separable potential

$$V_\ell(p,p') = g_\ell(p)\, g_\ell(p') - h_\ell(p)\, h_\ell(p') \quad ,$$

where the form factors are

$$g_\ell(p) = G_R \left[\frac{1}{\pi p^2}\, Q_\ell\left(1 + \frac{\mu_R^2}{2p^2}\right)\right]^{\frac{1}{2}} \qquad h_\ell(p) = G_A \left[\frac{1}{\pi p^2}\, Q_\ell\left(1 + \frac{\mu_A^2}{2p^2}\right)\right]^{\frac{1}{2}} ,$$

except in the partial waves $^1S_0$ and $^1P_1$, where the repulsive form factor is

$$g_\ell^R(p) = \frac{G_R p^2}{p^2 + \frac{\mu_R^2}{4}} \left[\frac{1}{\pi p^2}\, Q_\ell\left(1 + \frac{\mu_R^2}{2p^2}\right)\right]^{\frac{1}{2}} .$$

The units of the attractive inverse range μ_A and the repulsive inverse range μ_R are inverse fermis (F^{-1}, $1F = 10^{-13}$ cm). The units of the attractive coupling strength G_A and the repulsive coupling strength G_R are $(\text{MeV F})^{\frac{1}{2}}$. Dashes indicate that a form factor is to be set equal to zero. ΣR^2 is the sum of the squares of the residuals

$$\Sigma R^2 = \sum_{i=1}^{28} [\delta_\ell^{\text{expt}}(E_i) - \delta_\ell^{\text{fit}}(E_i)]^2 \quad ,$$

at the 28 data points in the range 0 to 400 MeV.

Table III (Continued).

Partial wave	Repulsive potential parameters $\mu_R(F^{-1})$	Repulsive potential parameters $G_R(\text{MeV F})^{\frac{1}{2}}$	Attractive potential parameters $\mu_A(F^{-1})$	Attractive potential parameters $G_A(\text{MeV F})^{\frac{1}{2}}$	ΣR^2
Singlet					
$^1S_0$	2.225[a]	20.84[a]	1.300	10.00	1538.4
$^1P_1$	0.644[a]	26.53[a]	1.256	31.53	44.22
$^1D_2$	-	-	1.415	10.61	1.952
$^1F_3$	0.933	12.06	-	-	2.304
$^1G_4$	-	-	0.936	6.539	0.032
Triplet					
$^3P_0$	1.799[a]	291.5[a]	1.475	26.65	158.9
$^3P_1$	0.477	167.1	3.268	21.00	71.86
$^3D_2$	5.663	108.5	1.057	15.40	11.16
$^3F_3$	0.674	5.545	-	-	0.051
$^3G_4$	-	-	0.799	9.513	0.050

[a] Special repulsive form factor must be used.

Table IV. Case IV fits to nucleon-nucleon phase shifts in uncoupled partial waves. These partial waves are fitted by the separable potential

$$V_\ell(p, p') = g_\ell(p)\, g_\ell(p') - h_\ell(p)\, h_\ell(p') \quad ,$$

where the form factors are

$$g_\ell(p) = C_R p^\ell/(p^2 + a_R^2)^{(\ell+1)}, \quad h_\ell(p) = C_A p^\ell/(p^2 + a_A^2)^{(\ell+1)} \quad .$$

The units of the attractive inverse range a_A and the repulsive inverse range a_R are inverse fermis (F^{-1}, $1F = 10^{-13}$ cm). The units of the attractive coupling strength C_A and the repulsive coupling strength C_R are $[\text{MeV } F^{-(2\ell+1)}]^{\frac{1}{2}}$. Dashes indicate that a form factor is to be set equal to zero. ΣR^2 is the sum of the square of the residuals

$$\Sigma R^2 \equiv \sum_{i=1}^{28} [\delta_\ell{}^{\text{expt}}(E_i) - \delta_\ell{}^{\text{fit}}(E_i)]^2 \quad ,$$

at the 28 data points in the range 0 to 400 MeV.

Table IV (Continued).

Partial wave	Repulsive potential parameters $a_R(F^{-1})$	Repulsive potential parameters $C_R[\text{MeV } F^{-(2\ell+1)}]^{\frac{1}{2}}$	Attractive potential parameters $a_A(F^{-1})$	Attractive potential parameters $C_A[\text{MeV } F^{-(2\ell+1)}]^{\frac{1}{2}}$	ΣR^2
Singlet					
$^1S_0$	6.157	302.0	1.786	27.33	456.3
$^1P_1$	1.967	121.6	1.566	49.73	25.31
$^1D_2$	-	-	2.721	530.5	11.95
$^1F_3$	2.341	1203.0	-	-	11.28
$^1G_4$	-	-	2.387	3378.0	0.507
Triplet					
$^3P_0$	5.000	1329.0	1.462	27.0	37.76
$^3P_1$	2.661	200.3	-	-	63.85
$^3D_2$	-	-	2.149	361.8	102.4
$^3F_3$	2.010	428.3	-	-	2.332
$^3G_4$	-	-	2.266	4881.0	9.605

Table V. Case I fits to nucleon-nucleon phase parameters in coupled partial waves. These partial waves are fitted by the separable potential

$$V_{\ell\ell'}(p, p') = (i^{\ell'-\ell})\,[g_\ell(p)\, g_{\ell'}(p') - h_\ell(p)\, h_{\ell'}(p')] \quad ,$$

where the form factors are

$$g_\ell(p) = C_\ell^R p^\ell / [p^2 + (a_\ell^R)^2]^{(\ell+1)/2} \quad ,$$

$$h_\ell(p) = C_\ell^A p^\ell / [p^2 + (a_\ell^A)^2]^{(\ell+1)/2} \quad .$$

The units of the attractive inverse ranges a^A_{J+1} and a^A_{J-1} and the repulsive inverse ranges a^R_{J+1} and a^R_{J-1} are inverse fermis (F^{-1}, $1F = 10^{-13}$ cm). The units of the attractive coupling strengths C^A_{J+1} and C^A_{J-1} and the repulsive coupling strengths C^R_{J+1} and C^R_{J-1} are $(\text{MeV F})^{\frac{1}{2}}$. Dashes indicate that a form factor is to be set equal to zero. ΣR^2 is the sum of the squares of the residuals,

$$\Sigma R^2 = \sum_{i=1}^{28} \{[\delta^{expt}_{J+1}(E_i) - \delta^{fit}_{J+1}(E_i)]^2 + [\epsilon^{expt}_J(E_i) - \epsilon^{fit}_J(E_i)]^2 + (\delta^{expt}_{J-1}(E_i) - \delta^{fit}_{J-1}(E_i)]^2\} \quad ,$$

at the 28 data points in the range 0 to 400 MeV.

Coupled wave system	Parameters for $\ell = J + 1$				Parameters for $\ell = J - 1$				ΣR^2
	Repulsive parameters		Attractive parameters		Repulsive parameters		Attractive parameters		
	$a^R_{J+1}(F^{-1})$	$C^R_{J+1}(\text{MeV F})^{\frac{1}{2}}$	$a^A_{J+1}(F^{-1})$	$C^A_{J+1}(\text{MeV F})^{\frac{1}{2}}$	$a^R_{J-1}(F^{-1})$	$C^R_{J-1}(\text{MeV F})^{\frac{1}{2}}$	$a^A_{J-1}(F^{-1})$	$C^A_{J-1}(\text{MeV F})^{\frac{1}{2}}$	
J = 1	0.848	20.38	0.744	10.82	3.990	22.98	0.982	9.804	1664.0
J = 2	-	-	0.342	0.467	-	-	1.509	5.345	5.526
J = 3	0.808	3.243	-	-	1.263	6.431	1.181	6.063	4.158
J = 4	-	-	0.737	1.018	-	-	1.466	3.440	0.807

UCRL-18501

Table VI. Case II fits to nucleon-nucleon phase parameters in coupled partial waves. These partial waves are fitted by the separable potential

$$V_{\ell\ell'}(p, p') = (i^{\ell'-\ell})[g_\ell(p)\, g_{\ell'}(p') - h_\ell(p)\, h_{\ell'}(p')] \quad ,$$

where the form factors are

$$g_\ell(p) = C_\ell^R p^\ell / [p^2 + (a_\ell^R)^2]^{(\ell+2)/2} \quad ,$$

$$h_\ell(p) = C_\ell^A p^\ell / [p^2 + (a_\ell^A)^2]^{(\ell+2)/2} \quad .$$

The units of the attractive inverse ranges a^R_{J+1} and a^A_{J-1} and the repulsive inverse ranges a^R_{J+1} and a^R_{J-1} are inverse fermis (F^{-1}, $1F = 10^{-13}$ cm). The units of the attractive coupling strengths C^A_{J+1} and C^A_{J-1} and the repulsive coupling strengths C^R_{J+1} and C^R_{J-1} are $(MeV/F)^{\frac{1}{2}}$. Dashes indicate that a form factor is to be set equal to zero. ΣR^2 is the sum of the squares of the residuals,

$$\Sigma R^2 = \sum_{i=1}^{28} \{[\delta^{expt}_{J+1}(E_i) - \delta^{fit}_{J+1}(E_i)]^2 + [\epsilon^{expt}_J(E_i) - \epsilon^{fit}_J(E_i)]^2 + [\delta^{expt}_{J-1}(E_i) - \delta^{fit}_{J-1}(E_i)]^2\} \quad ,$$

at the 28 data points in the range 0 to 400 MeV.

Coupled wave system	Parameters for $\ell = J+1$				Parameters for $\ell = J-1$				ΣR^2
	Repulsive parameters		Attractive parameters		Repulsive parameters		Attractive parameters		
	$a^R_{J+1}(F^{-1})$	$C^R_{J+1}(MeV/F)^{\frac{1}{2}}$	$a^A_{J+1}(F^{-1})$	$C^A_{J+1}(MeV/F)^{\frac{1}{2}}$	$a^R_{J-1}(F^{-1})$	$C^R_{J-1}(MeV/F)^{\frac{1}{2}}$	$a^A_{J-1}(F^{-1})$	$C^A_{J-1}(MeV/F)^{\frac{1}{2}}$	
J = 1	1.264	49.38	1.161	33.66	3.612	93.74	1.994	41.08	798.4
J = 2	-	-	0.652	1.102	-	-	2.198	24.24	5.765
J = 3	1.129	8.697	-	-	1.732	26.00	1.667	24.98	7.822
J = 4	-	-	1.033	3.270	-	-	1.884	14.78	0.960

UCRL-18501

Table VIII. Case IV fits to nucleon-nucleon phase parameters in coupled partial waves. These partial waves are fitted by the separable potential

$$V_{\ell\ell'}(p, p') = (i^{\ell'-\ell})[g_\ell(p)\, g_{\ell'}(p') - h_\ell(p)\, h_{\ell'}(p')] \ ,$$

where the form factors are

$$g_\ell(p) = C_\ell^R p^\ell / [p^2 + (a_\ell^R)^2]^{(\ell+1)} \ ,$$

$$h_\ell(p) = C_\ell^A p^\ell / [p^2 + (a_\ell^A)^2]^{(\ell+1)} \ .$$

The units of the attractive inverse ranges a^A_{J+1} and a^A_{J-1} and the repulsive inverse ranges a^R_{J+1} and a^R_{J-1} are inverse fermis (F^{-1}, $1F = 10^{-13}$ cm). The units of the attractive coupling strengths C^A_{J+1} and C^A_{J-1} and the repulsive coupling strengths C^R_{J+1} and C^R_{J-1} are $[\text{MeV } F^{-(2\ell+1)}]^{\frac{1}{2}}$. Dashes indicate that a form factor is to be set equal to zero. ΣR^2 is the sum of the squares of the residuals,

$$\Sigma R^2 = \sum_{i=1}^{28} \{[\delta^{\text{expt}}_{J+1}(E_i) - \delta^{\text{fit}}_{J+1}(E_i)]^2 + [\epsilon^{\text{expt}}_{J}(E_i) - \epsilon^{\text{fit}}_{J}(E_i)]^2 + [\delta^{\text{expt}}_{J-1}(E_i) - \delta^{\text{fit}}_{J-1}(E_i)]^2\} \ ,$$

at the 28 data points in the range 0 to 400 MeV.

Coupled wave system	Parameters for $\ell = J + 1$				Parameters for $\ell = J - 1$				ΣR^2
	Repulsive parameters		Attractive parameters		Repulsive parameters		Attractive parameters		
	$a^R_{J+1}(F^{-1})$	$C^R_{J+1}[\text{MeV } F^{-(2\ell+1)}]^{\frac{1}{2}}$	$a^A_{J+1}(F^{-1})$	$C^A_{J+1}[\text{MeV } F^{-(2\ell+1)}]^{\frac{1}{2}}$	$a^R_{J-1}(F^{-1})$	$C^R_{J-1}[\text{MeV } F^{-(2\ell+1)}]^{\frac{1}{2}}$	$a^A_{J-1}(F^{-1})$	$C^A_{J-1}[\text{MeV } F^{-(2\ell+1)}]^{\frac{1}{2}}$	
J = 1	1.738	477.4	1.633	318.2	3.472	85.53	2.000	40.92	1063.0
J = 2	-	-	1.289	24.33	-	-	2.731	123.9	8.056
J = 3	2.065	2151.0	-	-	2.331	465.1	2.287	449.4	18.17
J = 4	-	-	2.003	3007.0	-	-	2.805	1905.0	1.353

Table VII. Case III fits to nucleon-nucleon phase parameters in coupled partial waves. These partial waves are fitted by the separable potential

$$V_{\ell\ell'}(p, p') = (i^{\ell'-\ell})[g_\ell(p)\, g_{\ell'}(p') - h_\ell(p)\, h_{\ell'}(p')] \ ,$$

where the form factors are

$$g_\ell(p) = G_\ell^R \left\{ \frac{1}{\pi p^2} Q_\ell \left[1 + \frac{(\mu_\ell^R)^2}{2p^2} \right] \right\}^{\frac{1}{2}} \ ,$$

$$h_\ell(p) = G_\ell^A \left\{ \frac{1}{\pi p^2} Q_\ell \left[1 + \frac{(\mu_\ell^A)^2}{2p^2} \right] \right\}^{\frac{1}{2}} \ ,$$

where $Q_\ell(x)$ is the Legendre function of the second kind. In the $J = 1$ system, the repulsive form factor for $J - 1 (\ell = 0)$ is

$$g_\ell^R(p) = \left[\frac{G_\ell^R p^2}{p^2 + (\mu_\ell^R)^2/4} \right] \left\{ \frac{1}{\pi p^2} Q_\ell \left[1 + \frac{(\mu_\ell^R)^2}{2p^2} \right] \right\}^{\frac{1}{2}} \ .$$

The units of the attractive inverse ranges μ_{J+1}^A and μ_{J-1}^A and the repulsive inverse ranges μ_{J+1}^R and μ_{J-1}^R are inverse fermis (F^{-1}, $1F = 10^{-13}$ cm). The units of the attractive coupling strength G_{J+1}^A and G_{J-1}^A and the repulsive coupling strengths G_{J+1}^R and G_{J-1}^R are $(\text{MeV F})^{\frac{1}{2}}$. Dashes indicate that a form factor is to be set equal to zero. ΣR^2 is the sum of the squares of the residuals,

$$\Sigma R^2 = \sum_{i=1}^{28} \{[\delta_{J+1}^{\text{expt}}(E_i) - \delta_{J+1}^{\text{fit}}(E_i)]^2 + [\epsilon_J^{\text{expt}}(E_i) - \epsilon_J^{\text{fit}}(E_i)]^2 + [\delta_{J-1}^{\text{expt}}(E_i) - \delta_{J-1}^{\text{fit}}(E_i)]^2\} \ ,$$

at the 28 data points in the range 0 to 400 MeV.

Coupled wave system	Parameters for $\ell = J + 1$				Parameters for $\ell = J - 1$				ΣR^2
	Repulsive parameters		Attractive parameters		Repulsive parameters		Attractive parameters		
	$\mu_{J+1}^R(F^{-1})$	$G_{J+1}^R(\text{MeV F})^{\frac{1}{2}}$	$\mu_{J+1}^A(F^{-1})$	$G_{J+1}^A(\text{MeV F})^{\frac{1}{2}}$	$\mu_{J-1}^R(F^{-1})$	$G_{J-1}^R(\text{MeV F})^{\frac{1}{2}}$	$\mu_{J-1}^A(F^{-1})$	$G_{J-1}^A(\text{MeV F})^{\frac{1}{2}}$	
$J = 1$	0.592	77.49	0.511	18.10	3.249[a]	71.99[a]	1.458	13.94	2123.0
$J = 2$	-	-	0.142	0.577	-	-	1.601	9.750	10.62
$J = 3$	0.635	11.91	-	-	1.316	16.10	1.122	11.75	3.690
$J = 4$	-	-	0.521	2.344	-	-	1.481	9.864	0.708

[a] Special repulsive form factor must be used.

Table IX. Case I fits to nucleon-nucleon phase shifts in coupled waves, assuming $\epsilon_J = 0$ and neglecting δ_{J+1}. These partial waves are fitted by the separable potential

$$V_\ell(p,p') = g_\ell(p)\, g_\ell(p') - h_\ell(p)\, h_\ell(p') \quad ,$$

where the form factors are

$$g_\ell(p) = C_R p^\ell/(p^2 + a_R^2)^{(\ell+1)/2} \quad , \quad h_\ell(p) = C_A p^\ell/(p^2 + a_A^2)^{(\ell+1)/2} \quad .$$

The units of the attractive inverse range a_A and the repulsive inverse range a_R are inverse fermis (F^{-1}, $1F = 10^{-13}$ cm). The units of the attractive coupling strength C_A and the repulsive coupling strength C_R are $(\text{MeV F})^{\frac{1}{2}}$. Dashes indicate that a form factor is to be set equal to zero. ΣR^2 is the sum of the squares of the residuals

$$\Sigma R^2 = \sum_{i=1}^{28} [\delta_\ell{}^{\text{expt}}(E_i) - \delta_\ell{}^{\text{fit}}(E_i)]^2 \quad ,$$

at the 28 data points in the range 0 to 400 MeV.

Table IX (Continued).

Partial wave	Repulsive potential parameters		Attractive potential parameters		ΣR^2
	$a_R(F^{-1})$	$C_R(\text{MeV F})^{\frac{1}{2}}$	$a_A(F^{-1})$	$C_A(\text{MeV F})^{\frac{1}{2}}$	
$^3S_1$	2.335	82.73	2.068	72.84	50.51
$^3P_2$	-	-	1.509	5.349	0.406
$^3D_3$	4.427	345.3	1.259	3.403	0.128
$^3F_4$	-	-	1.530	3.663	0.068

Table X. Case II fits to nucleon-nucleon phase shifts in coupled waves, assuming $\epsilon_J = 0$ and neglecting δ_{J+1}. These partial waves are fitted by the separable potential

$$V_\ell(p,p') = g_\ell(p)\, g_\ell(p') - h_\ell(p)\, h_\ell(p') \quad ,$$

where the form factors are

$$g_\ell(p) = C_R p^\ell/(p^2 + a_R^2)^{(\ell+2)/2}, \quad h_\ell(p) = C_A p^\ell/(p^2 + a_A^2)^{(\ell+2)/2} \quad .$$

The units of the attractive inverse range a_A and the repulsive inverse range a_R are inverse fermis (F^{-1}, $1F = 10^{-13}$ cm). The units of the attractive coupling strength C_A and the repulsive coupling strength C_R are $(\mathrm{MeV/F})^{\frac{1}{2}}$. Dashes indicate that a form factor is to be set equal to zero. ΣR^2 is the sum of the squares of the residuals

$$\Sigma R^2 \equiv \sum_{i=1}^{28} [\delta_\ell^{\mathrm{expt}}(E_i) - \delta_\ell^{\mathrm{fit}}(E_i)]^2 \quad ,$$

at the 28 data points in the range 0 to 400 MeV.

Table X (Continued).

Partial wave	Repulsive potential parameters		Attractive potential parameters		ΣR^2
	$a_R(F^{-1})$	$C_R(MeV/F)^{\frac{1}{2}}$	$a_A(F^{-1})$	$C_A(MeV/F)^{\frac{1}{2}}$	
$^3S_1$	4.540	127.4	1.908	35.02	60.63
$^3P_2$	-	-	2.192	24.14	4.015
$^3D_3$	6.558	493.8	1.451	7.716	0.189
$^3F_4$	-	-	1.945	15.93	0.129

Table XI. Case III fits to nucleon-nucleon phase shifts in coupled waves, assuming $\epsilon_J = 0$ and neglecting δ_{J+1}. These partial waves are fitted by the separable potential

$$V_\ell(p,p') = g_\ell(p)\, g_\ell(p') - h_\ell(p)\, h_\ell(p') \quad ,$$

where the form factors are

$$g_\ell(p) = G_R \left[\frac{1}{\pi p^2} \, Q_\ell \left(1 + \frac{\mu_R^2}{2p^2} \right) \right]^{\frac{1}{2}}, \quad h_\ell(p) = G_A \left[\frac{1}{\pi p^2} \, Q_\ell \left(1 + \frac{\mu_A^2}{2p^2} \right) \right]^{\frac{1}{2}} ,$$

except in the fits to the partial wave $^3S_1$, where the repulsive form factor is

$$g_\ell^R(p) = \left[G_R p^2 / \left(p^2 + \frac{\mu_R^2}{4} \right) \right] \left[\frac{1}{\pi p^2} \, Q_\ell \left(1 + \frac{\mu_R^2}{2p^2} \right) \right]^{\frac{1}{2}} .$$

The units of the attractive inverse range μ_A and the repulsive inverse range μ_R are inverse fermis (F^{-1}, $1F = 10^{-13}$ cm). The units of the attractive coupling strength G_A and the repulsive coupling strength G_R are $(\text{MeV F})^{\frac{1}{2}}$. Dashes indicate that a form factor is to be set equal to zero. ΣR^2 is the sum of the squares of the residuals

$$\Sigma R^2 \equiv \sum_{i=1}^{28} [\delta_\ell^{\text{expt}}(E_i) - \delta_\ell^{\text{fit}}(E_i)]^2 \quad ,$$

at the 28 data points in the range 0 to 400 MeV.

Table XI (Continued).

Partial wave	Repulsive potential parameters		Attractive potential parameters		ΣR^2
	$\mu_R(F^{-1})$	$G_R(\text{MeV F})^{\frac{1}{2}}$	$\mu_A(F^{-1})$	$G_A(\text{MeV F})^{\frac{1}{2}}$	
$^3S_1$	3.441[a]	777.4[a]	3.259	29.97	545.9
$^3P_2$	-	-	1.600	9.764	2.622
$^3D_3$	3.025	872.8	2.543	98.48	0.148
$^3F_4$	-	-	1.581	10.83	0.010

[a] Special repulsive form factor must be used.

Table XII. Case IV fits to nucleon-nucleon phase shifts in coupled waves, assuming $\epsilon_J = 0$ and neglecting δ_{J+1}. These partial waves are fitted by the separable potential

$$V_\ell(p,p') = g_\ell(p)\, g_\ell(p') - h_\ell(p)\, h_\ell(p') \quad ,$$

where the form factors are

$$g_\ell(p) = C_R p^\ell/(p^2 + a_R^2)^{(\ell+1)} \quad , \quad h_\ell(p) = C_A p^\ell/(p^2 + a_A^2)^{(\ell+1)} \quad .$$

The units of the attractive inverse range a_A and the repulsive inverse range a_R are inverse fermis (F^{-1}, $1F = 10^{-13}$ cm). The units of the attractive coupling strength C_A and the repulsive coupling strength C_R are $[\text{MeV } F^{-(2\ell+1)}]^{\frac{1}{2}}$. Dashes indicate that a form factor is to be set equal to zero. ΣR^2 is the sum of the squares of the residuals

$$\Sigma R^2 = \sum_{i=1}^{28} [\delta_\ell{}^{\text{expt}}(E_i) - \delta_\ell{}^{\text{fit}}(E_i)]^2 \quad ,$$

at the 28 data points in the range 0 to 400 MeV.

Table XII (Continued).

Partial wave	Repulsive potential parameters		Attractive potential parameters		ΣR^2
	$a_R(F^{-1})$	$C_R[\text{MeV } F^{-(2\ell+1)}]^{\frac{1}{2}}$	$a_A(F^{-1})$	$C_A[\text{MeV } F^{-(2\ell+1)}]^{\frac{1}{2}}$	
$^3S_1$	4.540	127.4	1.908	35.02	60.63
$^3P_2$	-	-	2.720	122.5	7.275
$^3D_3$	2.489	307.8	2.253	248.0	0.775
$^3F_4$	-	-	2.861	2115.0	0.237

Table XIII. Low-energy parameters.[a]

	$^1S_0$ parameters	
	Singlet scattering length a_s (fermis)	Singlet effective range r_s (fermis)
Experiment	-23.678	2.729
Case I	-23.678	2.729
Case II	-23.678	2.729
Case III	-23.681	2.722
Case IV	-23.678	2.729
	$^3S_1$ parameters (coupling to $^3D_1$ neglected)	
	Triplet scattering length a_t (fermis)	Triplet effective range r_t (fermis)
Experiment	5.396	1.726
Case I	5.345	1.724
Case II	5.396	1.726
Case III	5.399	1.730
Case IV	5.396	1.726

Table XIII (Continued).

	J = 1 parameters			
	Triplet scattering length a_t (fermis)	Triplet effective range r_t (fermis)	Deuteron quadrupole moment (F^2)	Deuteron D state probability (%)
Experiment	5.396	1.726	0.278	-
Case I	5.654	2.041	0.277	0.7
Case II	5.384	1.710	0.276	1.1
Case III	5.565	1.936	0.278	0.5
Case IV	5.380	1.705	0.274	1.4

[a] All fits to the partial waves $^1S_0$ contain a singlet antibound state pole at E = -0.0665 MeV on the second or unphysical sheet of the complex energy Riemann surface. All fits to the J = 1 coupled wave system and to the $^3S_1$ partial wave neglecting the coupling $^3D_1$ contain the deuteron pole at E = -2.22452 MeV on the physical sheet of the complex energy Riemann surface.

Table XIV. Maximum excursions of the error (fitted value minus data value) and the laboratory kinetic energies at which they occur.

Phase parameter	Maximum excursions of the error (degrees)			
	Case I	Case II	Case III	Case IV
$^1S_0$	10.04 at 400 MeV	10.58 at 5 MeV	15.83 at 400 MeV	10.58 at 5 MeV
	-1.639 at 160 MeV	-1.314 at 180 MeV	-8.684 at 70 MeV	-1.314 at 180 MeV
$^1P_1$	2.546 at 220 MeV	2.193 at 15 MeV	2.022 at 5 MeV	1.362 at 15 MeV
	-3.608 at 400 MeV	-1.669 at 90 MeV	-1.841 at 400 MeV	-2.220 at 400 MeV
$^1D_2$	0.482 at 220 MeV	0.586 at 220 MeV	0.295 at 200 MeV	0.695 at 240 MeV
	-0.729 at 400 MeV	-0.936 at 400 MeV	-0.438 at 400 MeV	-1.079 at 400 MeV
$^1F_3$	0.804 at 400 MeV	0.916 at 400 MeV	0.604 at 400 MeV	1.068 at 70 MeV
	-0.504 at 220 MeV	-0.580 at 240 MeV	-0.379 at 220 MeV	-0.643 at 240 MeV
$^1G_4$	0.085 at 240 MeV	0.109 at 260 MeV	0.042 at 240 MeV	0.147 at 260 MeV
	-0.129 at 400 MeV	-0.171 at 400 MeV	-0.065 at 400 MeV	-0.232 at 90 MeV
$^3P_0$	1.479 at 400 MeV	1.105 at 400 MeV	4.599 at 400 MeV	2.857 at 400 MeV
	-1.107 at 10 MeV	-1.067 at 10 MeV	-3.414 at 140 MeV	-1.031 at 10 MeV

Table XIV (Continued-1).

Phase parameter	Maximum excursions of the error (degrees)			
	Case I	Case II	Case III	Case IV
$^3P_1$	0.114 at 5 MeV	2.440 at 30 MeV	3.854 at 400 MeV	2.594 at 30 MeV
	-0.074 at 40 MeV	-1.419 at 200 MeV	-2.001 at 120 MeV	-1.482 at 220 MeV
$^3D_2$	1.355 at 400 MeV	1.516 at 140 MeV	1.818 at 400 MeV	2.341 at 160 MeV
	-1.264 at 30 MeV	-2.541 at 40 MeV	-0.848 at 220 MeV	-3.595 at 40 MeV
$^3F_3$	0.114 at 40 MeV	0.290 at 400 MeV	0.057 at 200 MeV	0.503 at 400 MeV
	-0.083 at 180 MeV	-0.200 at 200 MeV	-0.087 at 400 MeV	-0.319 at 220 MeV
$^3G_4$	0.276 at 220 MeV	0.436 at 220 MeV	0.040 at 220 MeV	0.632 at 260 MeV
	-0.427 at 400 MeV	-0.682 at 400 MeV	-0.093 at 400 MeV	-1.021 at 400 MeV
$^3S_1$	11.07 at 400 MeV	3.791 at 380 MeV	14.37 at 400 MeV	2.764 at 340 MeV
	-9.099 at 50 MeV	-3.513 at 70 MeV	-5.455 at 40 MeV	-3.536 at 70 MeV
ϵ_1	3.904 at 400 MeV	7.891 at 400 MeV	1.803 at 400 MeV	7.877 at 400 MeV
	-4.132 at 20 MeV	-5.371 at 40 MeV	-3.364 at 5 MeV	-6.505 at 60 MeV
$^3D_1$	6.501 at 400 MeV	5.127 at 400 MeV	11.54 at 400 MeV	8.723 at 400 MeV
	-1.647 at 160 MeV	-2.838 at 220 MeV	-2.100 at 40 MeV	-3.682 at 200 MeV

Table XIV (Continued-2).

Phase parameter	Maximum excursions of the error (degrees)			
	Case I	Case II	Case III	Case IV
$^3P_2$	0.201 at 120 MeV	0.462 at 180 MeV	0.754 at 400 MeV	0.620 at 180 MeV
	-0.194 at 30 MeV	-0.599 at 40 MeV	-0.422 at 200 MeV	-0.778 at 40 MeV
ϵ_2	0.463 at 140 MeV	0.250 at 180 MeV	0.628 at 140 MeV	0.375 at 30 MeV
	-1.024 at 400 MeV	-0.651 at 400 MeV	-1.175 at 400 MeV	0.247 at 400 MeV
$^3F_2$	0.325 at 400 MeV	0.269 at 50 MeV	0.350 at 400 MeV	0.219 at 80 MeV
	-0.239 at 180 MeV	-0.205 at 200 MeV	-0.270 at 160 MeV	-0.173 at 220 MeV
$^3D_3$	0.602 at 400 MeV	0.401 at 400 MeV	0.746 at 400 MeV	0.233 at 400 MeV
	-0.313 at 240 MeV	-0.190 at 260 MeV	-0.465 at 220 MeV	-0.157 at 300 MeV
ϵ_3	0.315 at 200 MeV	0.556 at 200 MeV	0.073 at 380 MeV	0.813 at 240 MeV
	-0.535 at 50 MeV	-0.852 at 60 MeV	-0.175 at 60 MeV	-1.306 at 70 MeV
$^3G_3$	0.267 at 400 MeV	0.363 at 400 MeV	0.167 at 400 MeV	0.436 at 400 MeV
	-0.172 at 120 MeV	-0.190 at 200 MeV	-0.231 at 80 MeV	-0.262 at 260 MeV
$^3F_4$	0.107 at 240 MeV	0.128 at 240 MeV	0.080 at 200 MeV	0.144 at 280 MeV
	-0.145 at 400 MeV	-0.174 at 400 MeV	-0.086 at 400 MeV	-0.220 at 400 MeV

Table XIV (Continued-3).

Phase parameter	Maximum excursions of the error (degrees)			
	Case I	Case II	Case III	Case IV
ϵ_4	0.215 at 100 MeV	0.249 at 100 MeV	0.210 at 140 MeV	0.327 at 100 MeV
	-0.061 at 400 MeV	-0.011 at 400 MeV	-0.117 at 400 MeV	-0.013 at 320 MeV
$^3H_4$	0.172 at 140 MeV	0.188 at 180 MeV	0.154 at 140 MeV	0.197 at 220 MeV
	-0.110 at 400 MeV	-0.149 at 400 MeV	-0.071 at 400 MeV	-0.210 at 400 MeV

Table XV. Maximum excursions of the error (fitted value minus data value) and the laboratory kinetic energies at which they occur, for the phase shifts in coupled waves, assuming $\epsilon_J = 0$ and neglecting δ_{J+1}.

Phase parameter	Maximum excursion of the error (degrees)			
	Case I	Case II	Case III	Case IV
$^3S_1$	0.800 at 340 MeV	0.923 at 320 MeV	8.470 at 400 MeV	0.923 at 320 MeV
	-2.393 at 60 MeV	-2.571 at 60 MeV	-1.693 at 50 MeV	-2.571 at 60 MeV
$^3P_2$	0.164 at 120 MeV	0.505 at 180 MeV	0.786 at 400 MeV	0.665 at 180 MeV
	-0.228 at 30 MeV	-0.619 at 40 MeV	-0.411 at 200 MeV	-0.800 at 40 MeV
$^3D_3$	0.224 at 400 MeV	0.218 at 400 MeV	0.227 at 400 MeV	0.623 at 400 MeV
	-0.102 at 220 MeV	-0.115 at 260 MeV	-0.098 at 220 MeV	-0.138 at 220 MeV
$^3F_4$	0.060 at 280 MeV	0.082 at 280 MeV	0.021 at 240 MeV	0.114 at 280 MeV
	-0.091 at 400 MeV	-0.128 at 400 MeV	-0.036 at 400 MeV	-0.169 at 400 MeV

UCRL-18501

Table XVI. Grand total of the sum of the squares of the residuals for all uncoupled waves and coupled wave systems through $J = 4$.

	Sum of squares of residuals
Case I	2263.7
Case II	1445.5
Case III	3966.9
Case IV	1811.9

FIGURE CAPTIONS

Fig. 1. Fits to the singlet phase shift $^1S_0$. The curve marked Δ is the data value of the phase parameter in degrees and is read with the left-hand scale. The other curves are the absolute error (fitted value minus data value) in degrees of the various fits and are read with the right-hand scale. The dashed curve represents the Case I fit, the solid curve marks the Case II and Case IV fits, and the dotted curve indicates the Case III fit.

Fig. 2. Fits to the singlet phase shift $^1P_1$. The curve marked Δ is the data value of the phase parameter in degrees and is read with the left-hand scale. The other curves are the absolute error (fitted value minus data value) and are read with the right-hand scale. The dashed curve represents the Case I fit, the solid curve marks the Case II fit, the dotted curve indicates the Case III fit and the dot-dash curve denotes the Case IV fit.

Fig. 3. Fits to the singlet phase shift $^1D_2$. Description of curves is as for Fig. 2.

Fig. 4. Fits to the singlet phase shift $^1F_3$. Description of curves is as for Fig. 2.

Fig. 5. Fits to the singlet phase shift $^1G_4$. Description of curves is as for Fig. 2.

Fig. 6. Fits to the (uncoupled) triplet phase shift $^3P_0$. Description of curves is as for Fig. 2.

Fig. 7. Fits to the (uncoupled) triplet phase shift $^3P_1$. Description of curves is as for Fig. 2.

Fig. 8. Fits to the (uncoupled) triplet phase shift $^3D_2$. Description of curves is as for Fig. 2.

Fig. 9. Fits to the (uncoupled) triplet phase shift $^3F_3$. Description of curves is as for Fig. 2.

Fig. 10. Fits to the uncoupled triplet phase shift $^3G_4$. Description of curves is as for Fig. 2.

Fig. 11. Fits to the triplet phase shift $^3S_1$ ($J = 1$ coupled waves). Description of curves is as for Fig. 2.

Fig. 12. Fits to the triplet mixing parameter ϵ_1 ($J = 1$ coupled waves). Description of curves is as for Fig. 2.

Fig. 13. Fits to the triplet phase shift $^3D_1$ ($J = 1$ coupled waves). Description of curves is as for Fig. 2.

Fig. 14. Fits to the triplet phase shift $^3P_2$ ($J = 2$ coupled waves). Description of curves is as for Fig. 2.

Fig. 15. Fits to the triplet mixing parameters ϵ_2 ($J = 2$ coupled waves). Description of curves is as for Fig. 2.

Fig. 16. Fits to the triplet phase shift $^3F_2$ ($J = 2$ coupled waves). Description of curves is as for Fig. 2.

Fig. 17. Fits to the triplet phase shift $^3D_3$ ($J = 3$ coupled waves). Description of curves is as for Fig. 2.

Fig. 18. Fits to the triplet mixing parameter ϵ_3 ($J = 3$ coupled waves). Description of curves is as for Fig. 2.

Fig. 19. Fits to the triplet phase shift $^3G_3$ ($J = 3$ coupled waves). Description of curves is as for Fig. 2.

Fig. 20. Fits to the triplet phase shift $^3F_4$ ($J = 4$ coupled waves). Description of curves is as for Fig. 2.

Fig. 21. Fits to the triplet mixing parameter ϵ_4 ($J = 4$ coupled waves). Description of curves is as for Fig. 2.

Fig. 22. Fits to the triplet phase shift $^3H_4$ ($J = 4$ coupled waves). Description of curves is as for Fig. 2.

Fig. 23. Fits to the triplet phase shift $^3S_1$ (assuming $\epsilon_1 = 0$ and neglecting δ^3D_1). Description of curves is as for Fig. 1.

Fig. 24. Fits to the triplet phase shift $^3P_2$ (assuming $\epsilon_2 = 0$ and neglecting δ^3F_2). Description of curves is as for Fig. 2.

Fig. 25. Fits to the triplet phase shift $^3D_3$ (assuming $\epsilon_3 = 0$ and neglecting δ^3G_3). Description of curves is as for Fig. 2.

Fig. 26. Fits to the triplet phase shift $^3F_4$ (assuming $\epsilon_4 = 0$ and Neglecting δ^3H_4). Description of curves is as for Fig. 2.

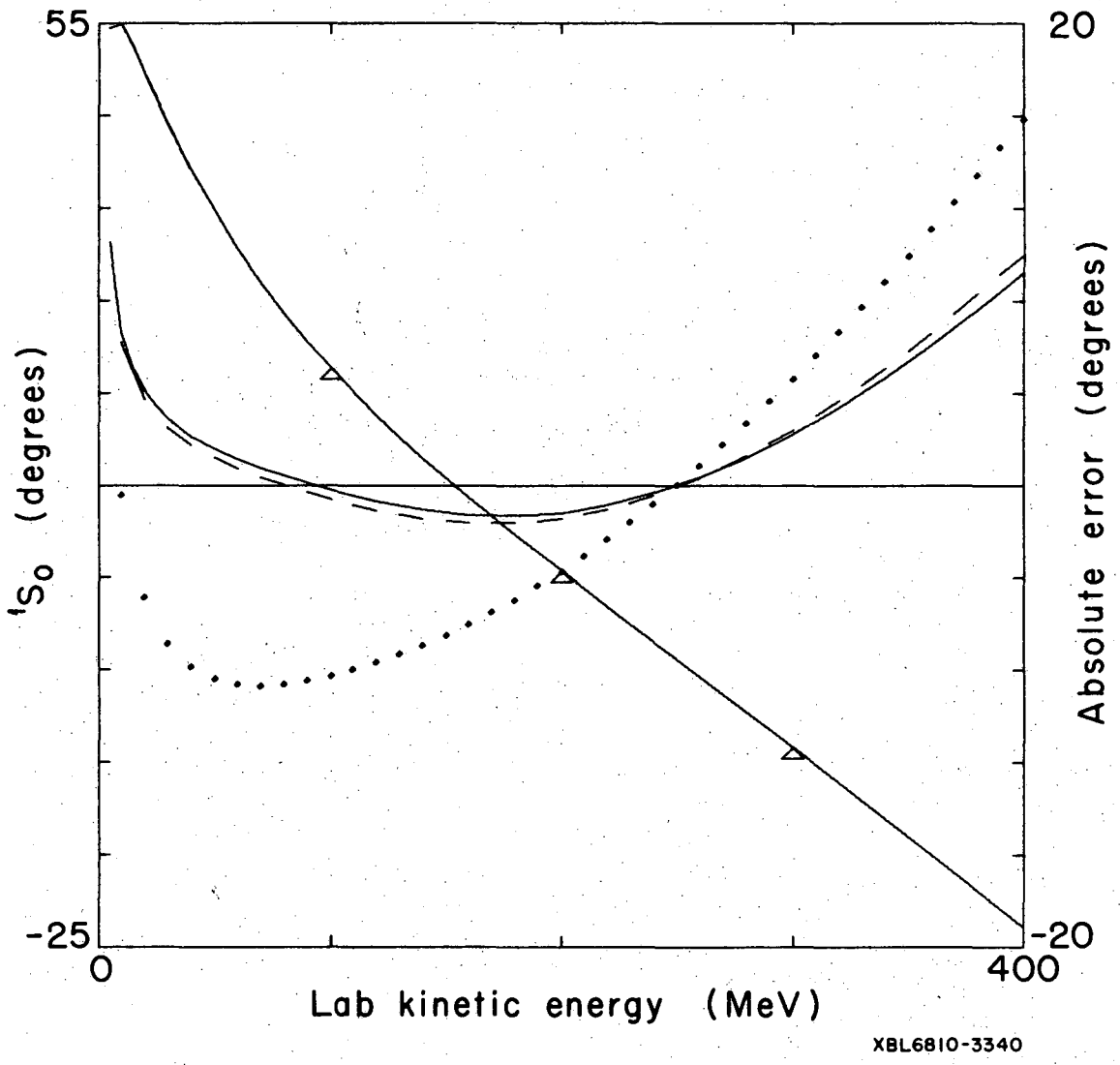
55
20
-25
-20
0
400
$^1S_0$ (degrees)
Absolute error (degrees)
Lab kinetic energy (MeV)
XBL6810-3340

Fig. 1

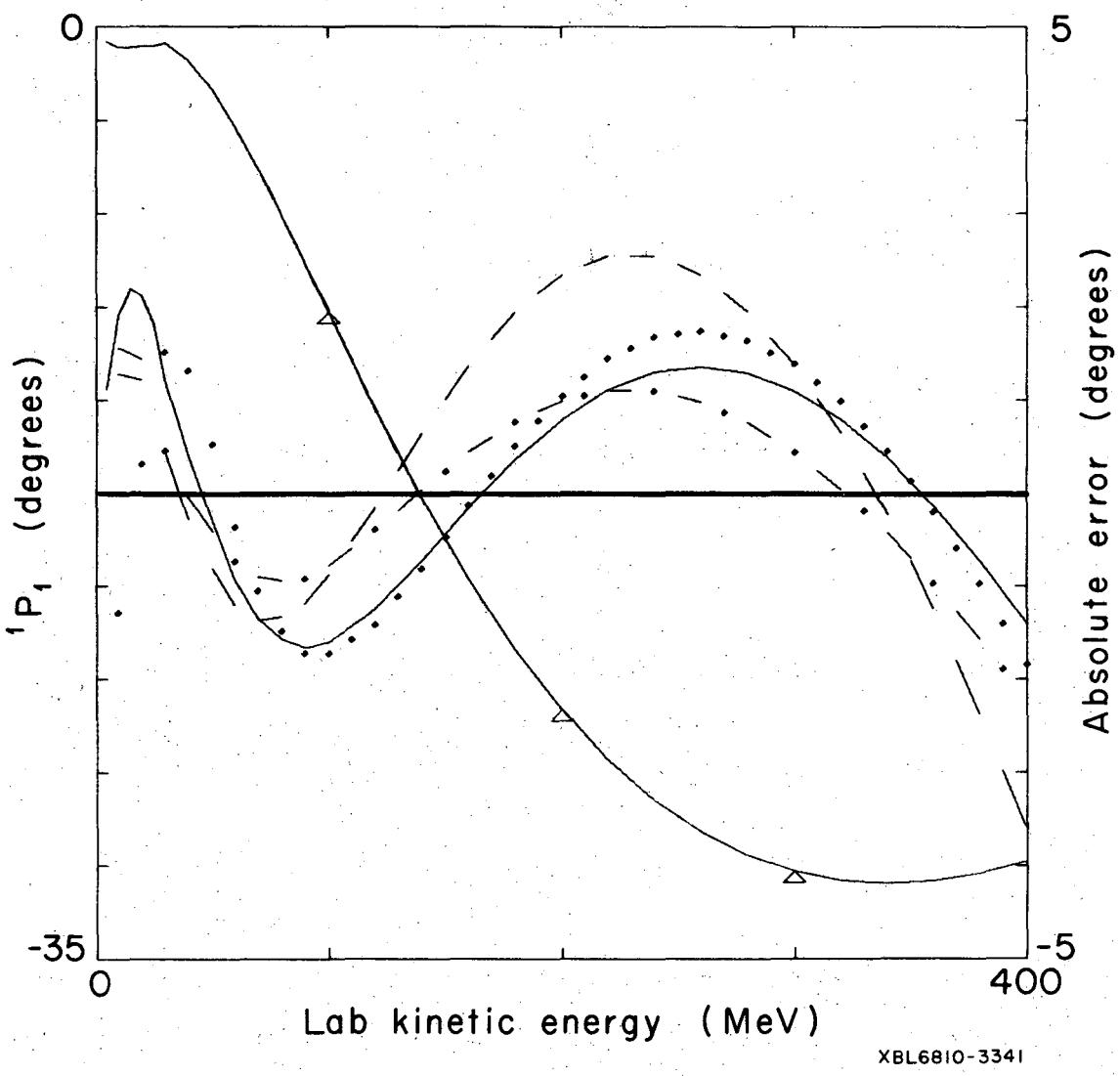
0
5
$^1P_1$ (degrees)
Absolute error (degrees)
-35
-5
0
400
Lab kinetic energy (MeV)
XBL6810-3341

Fig. 2

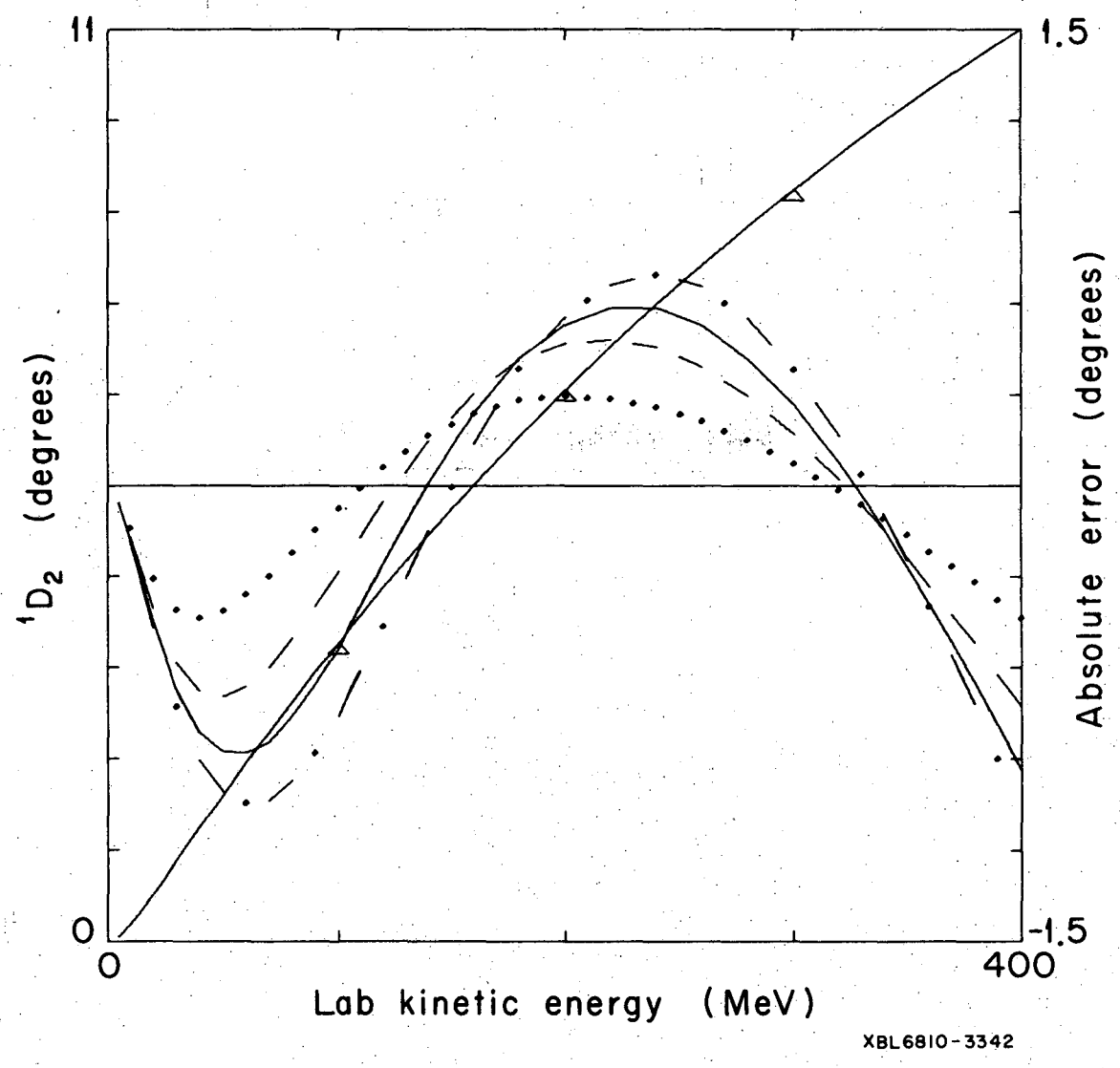
11
0
1.5
-1.5
0
400
$^1D_2$ (degrees)
Absolute error (degrees)
Lab kinetic energy (MeV)
XBL6810-3342

Fig. 3

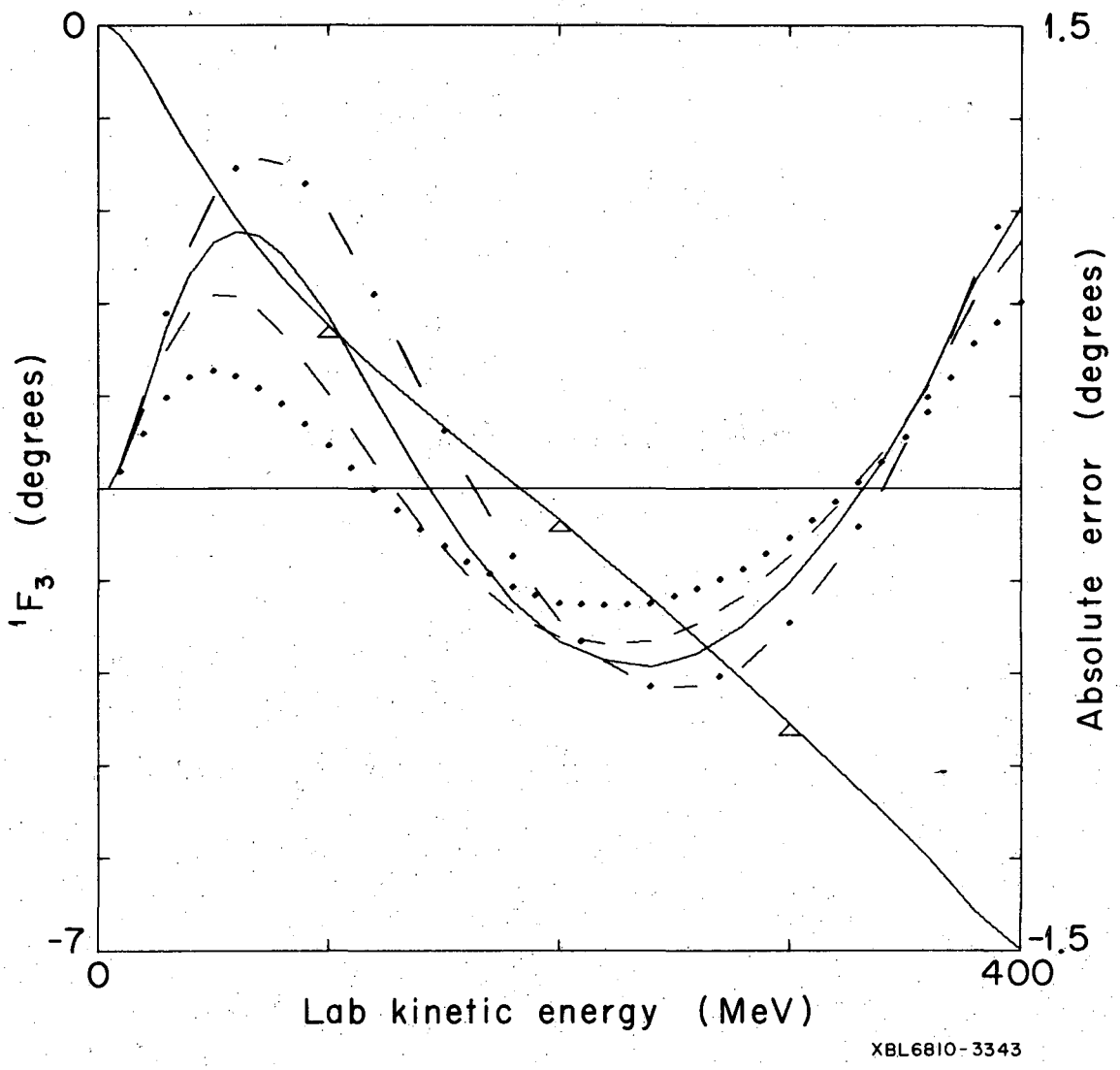
0
1.5
$^1F_3$ (degrees)
Absolute error (degrees)
-7
-1.5
0
400
Lab kinetic energy (MeV)
XBL6810-3343

Fig. 4

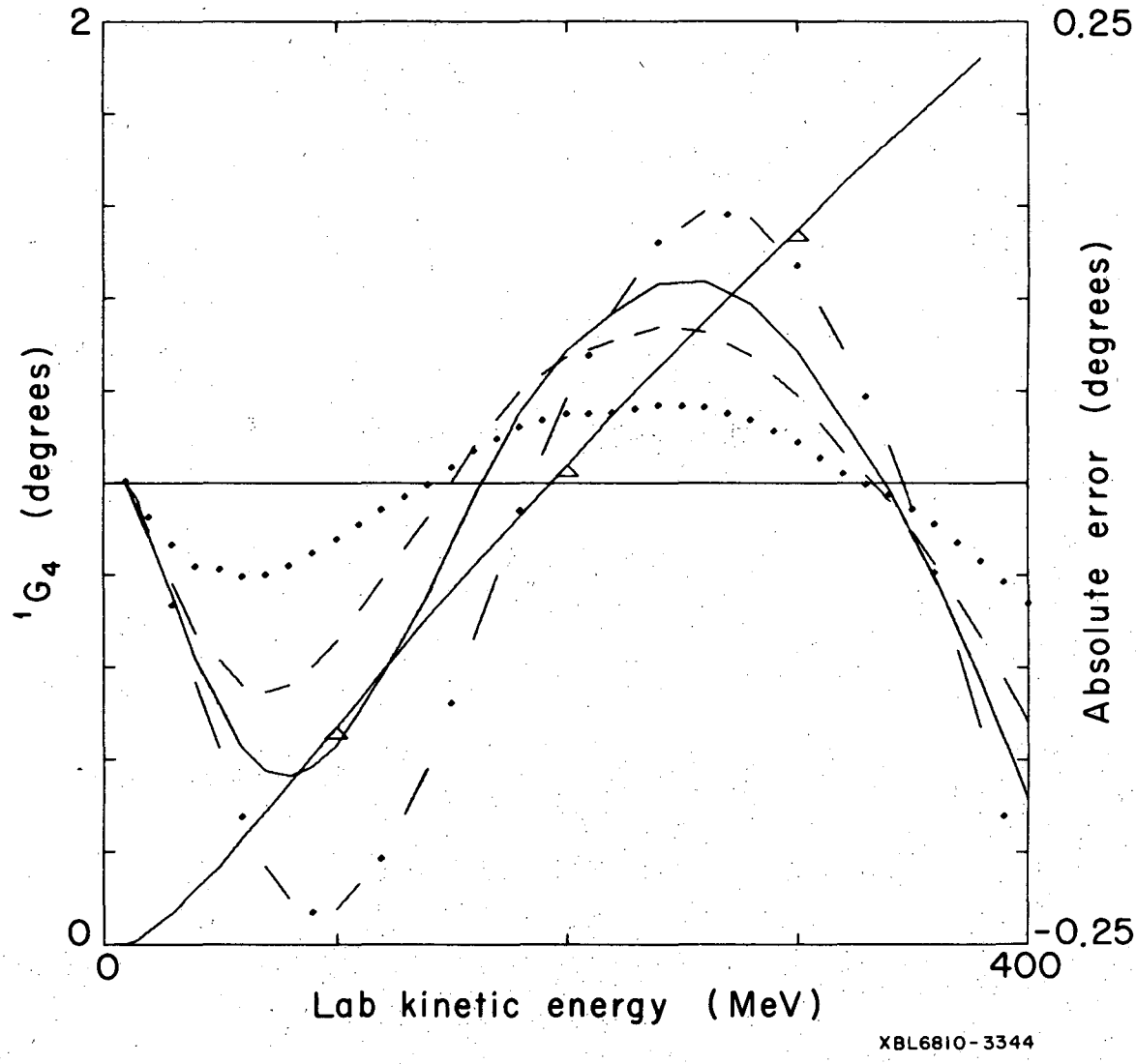
2
0
0.25
-0.25
0
400
$^1G_4$ (degrees)
Absolute error (degrees)
Lab kinetic energy (MeV)
XBL6810-3344

Fig. 5

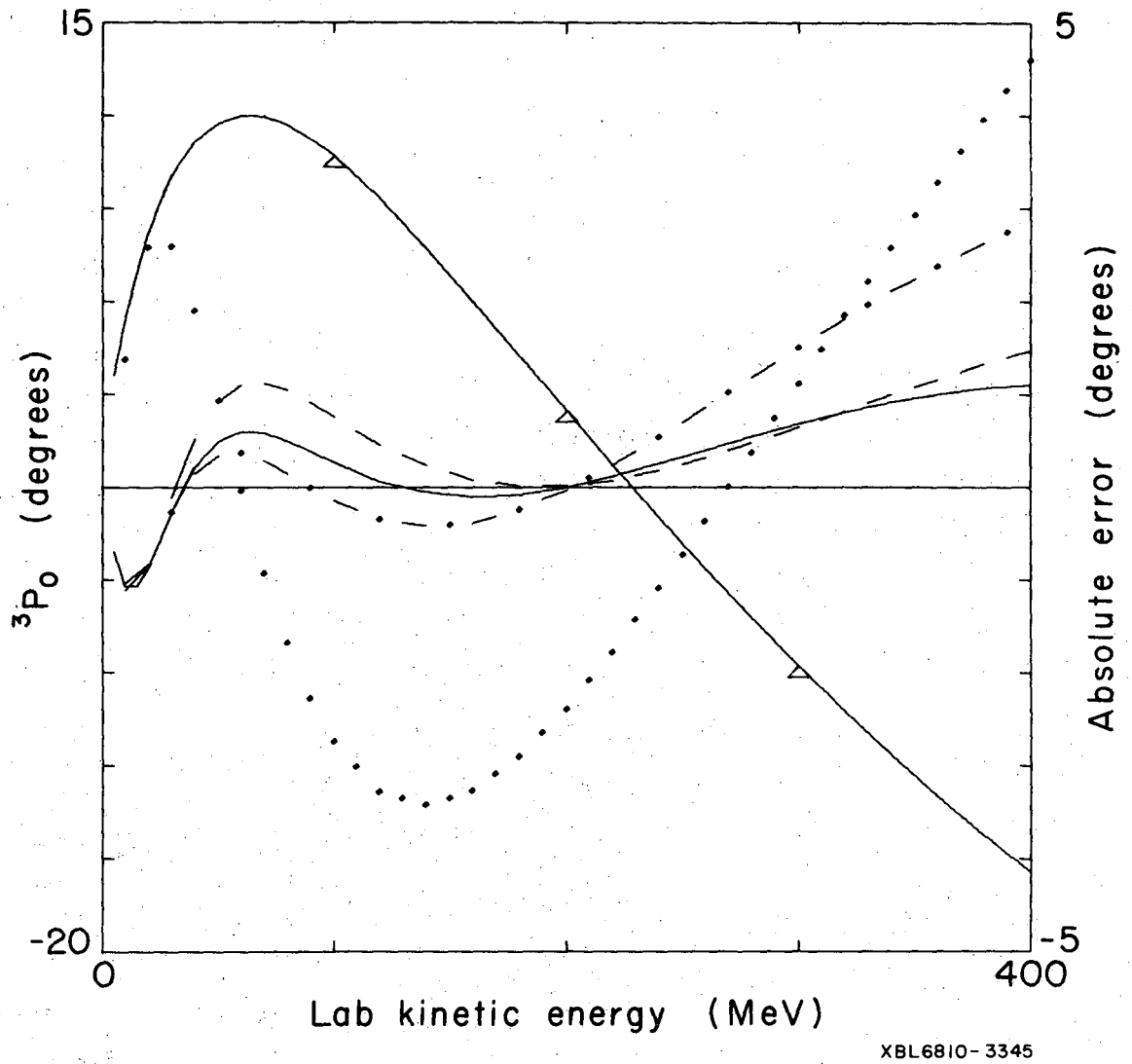
15
5
-20
-5
0
400
$^3P_0$ (degrees)
Absolute error (degrees)
Lab kinetic energy (MeV)
XBL6810-3345

Fig. 6

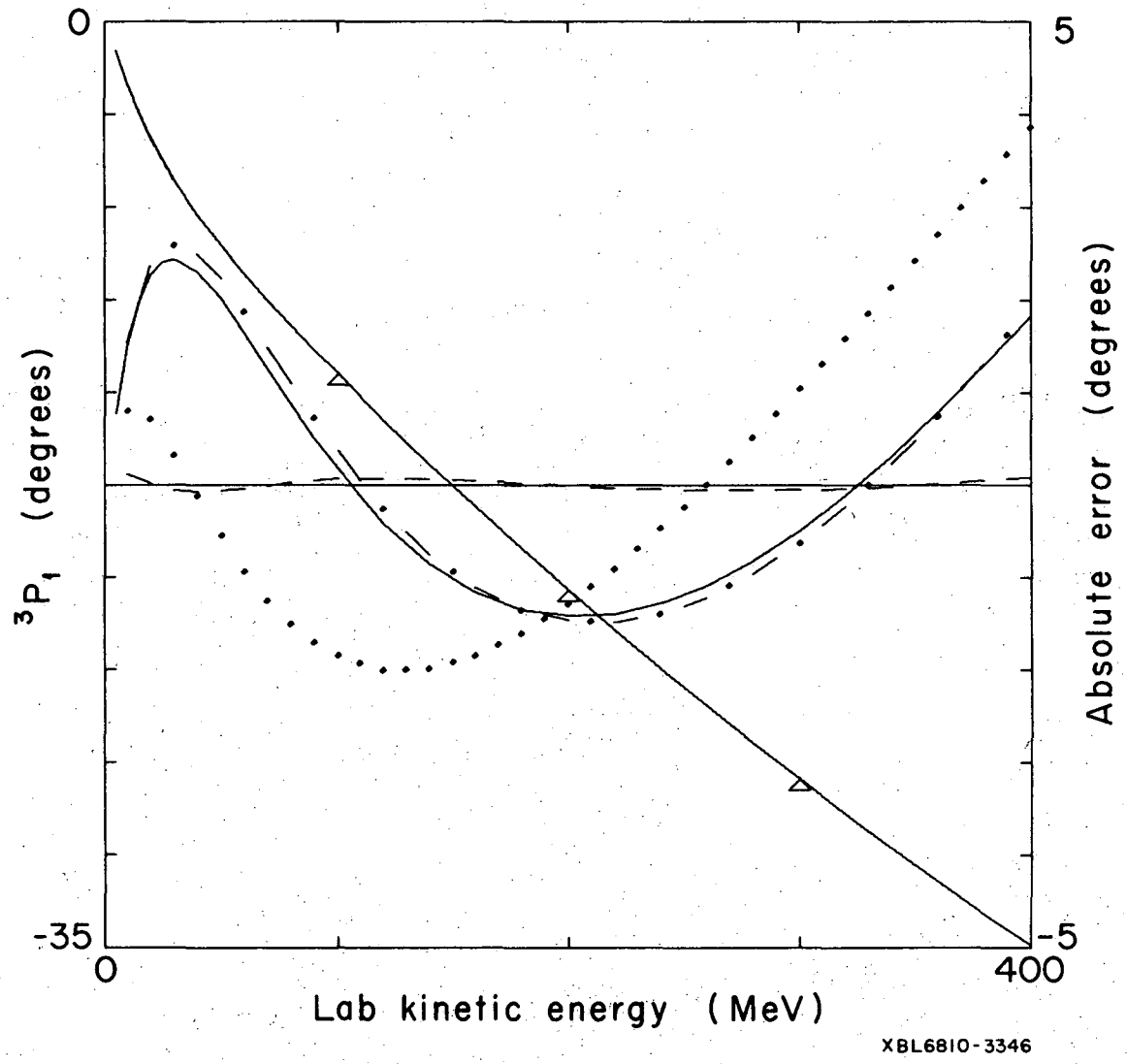
0
5
$^3P_1$ (degrees)
Absolute error (degrees)
-35
-5
0
400
Lab kinetic energy (MeV)
XBL6810-3346

Fig. 7

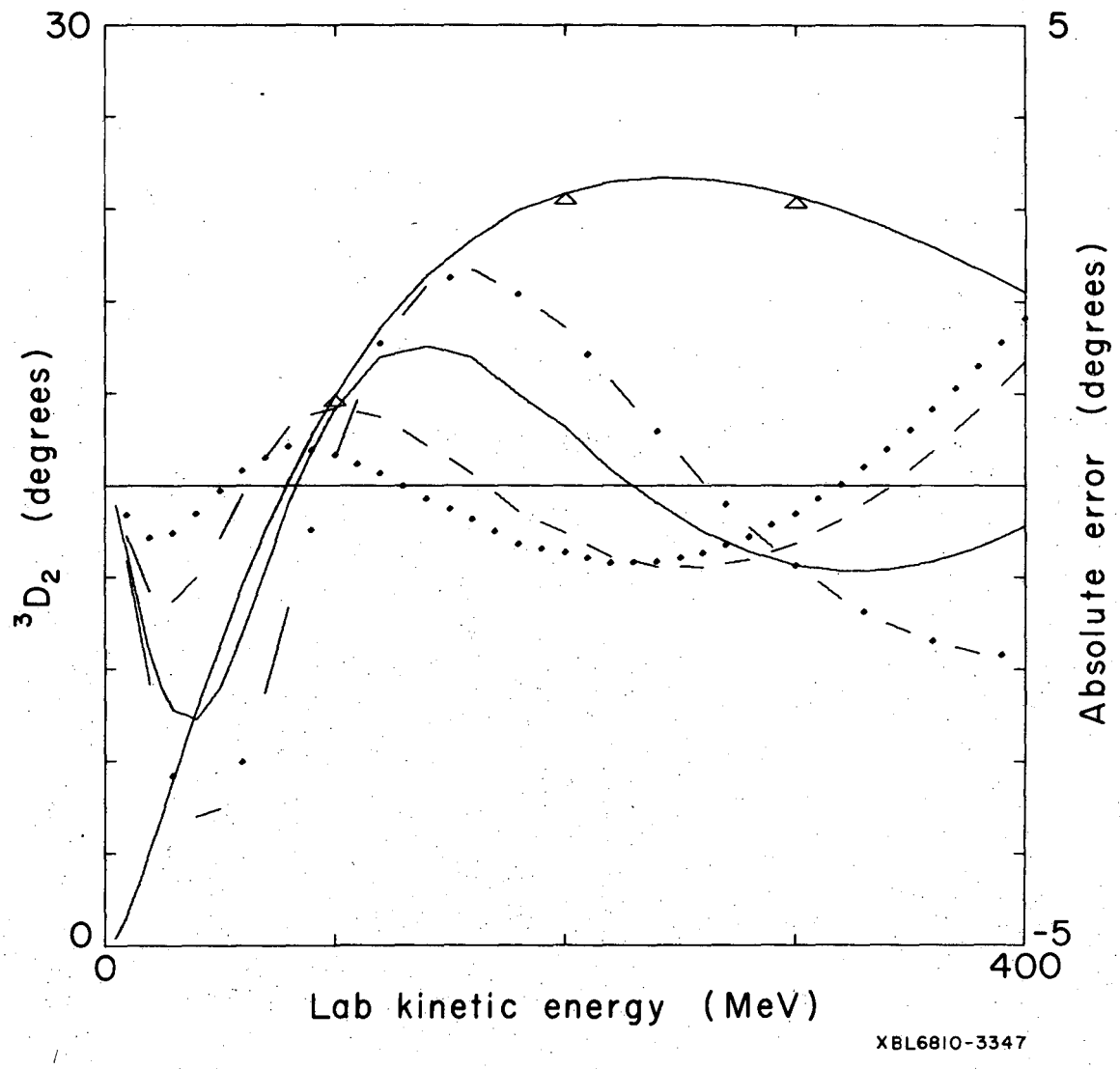
30
5
0
-5
0
400
$^3D_2$ (degrees)
Absolute error (degrees)
Lab kinetic energy (MeV)
XBL6810-3347

Fig. 8

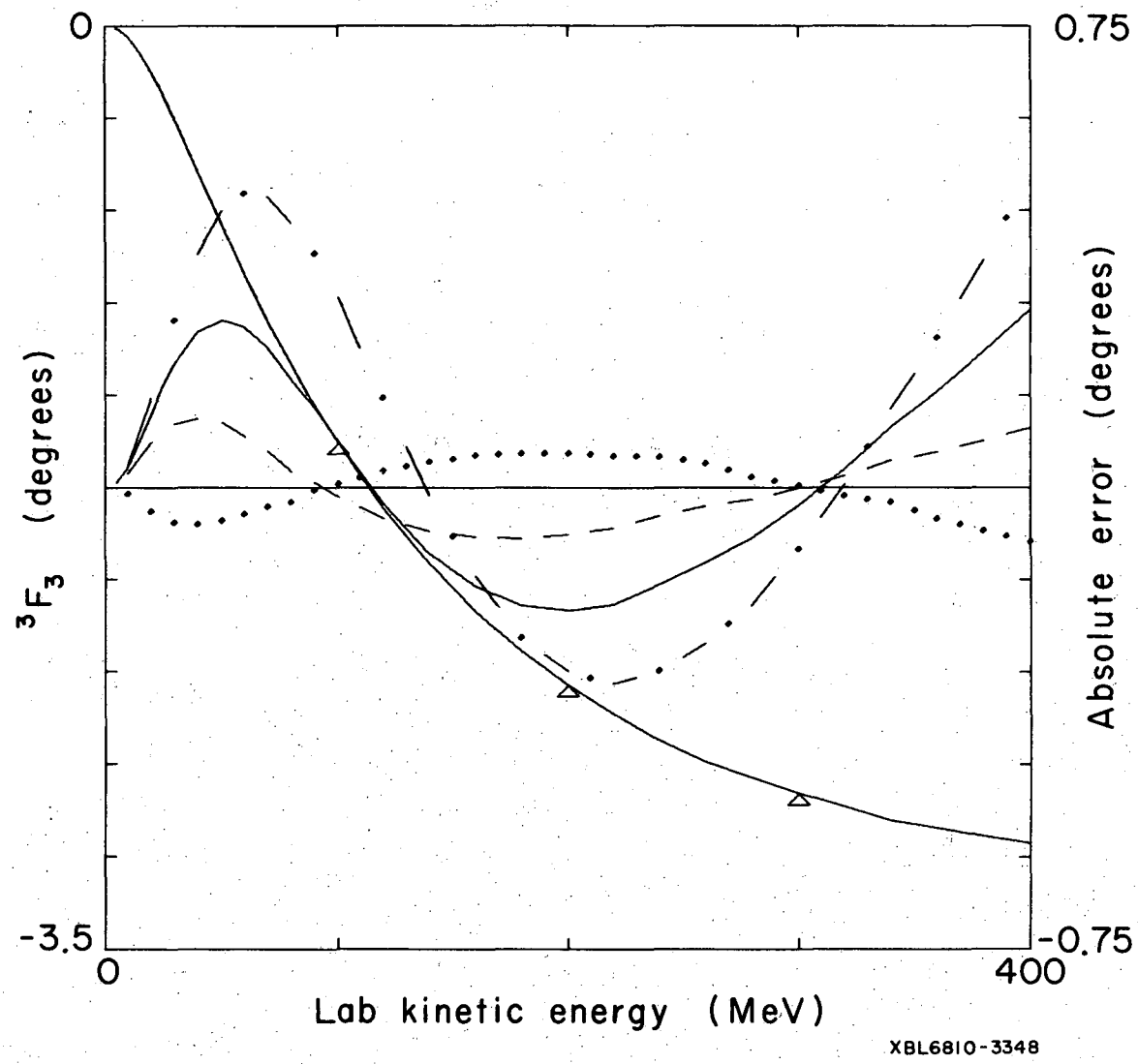
0
0.75
$^3F_3$ (degrees)
Absolute error (degrees)
-3.5
-0.75
0
400
Lab kinetic energy (MeV)
XBL6810-3348

Fig. 9

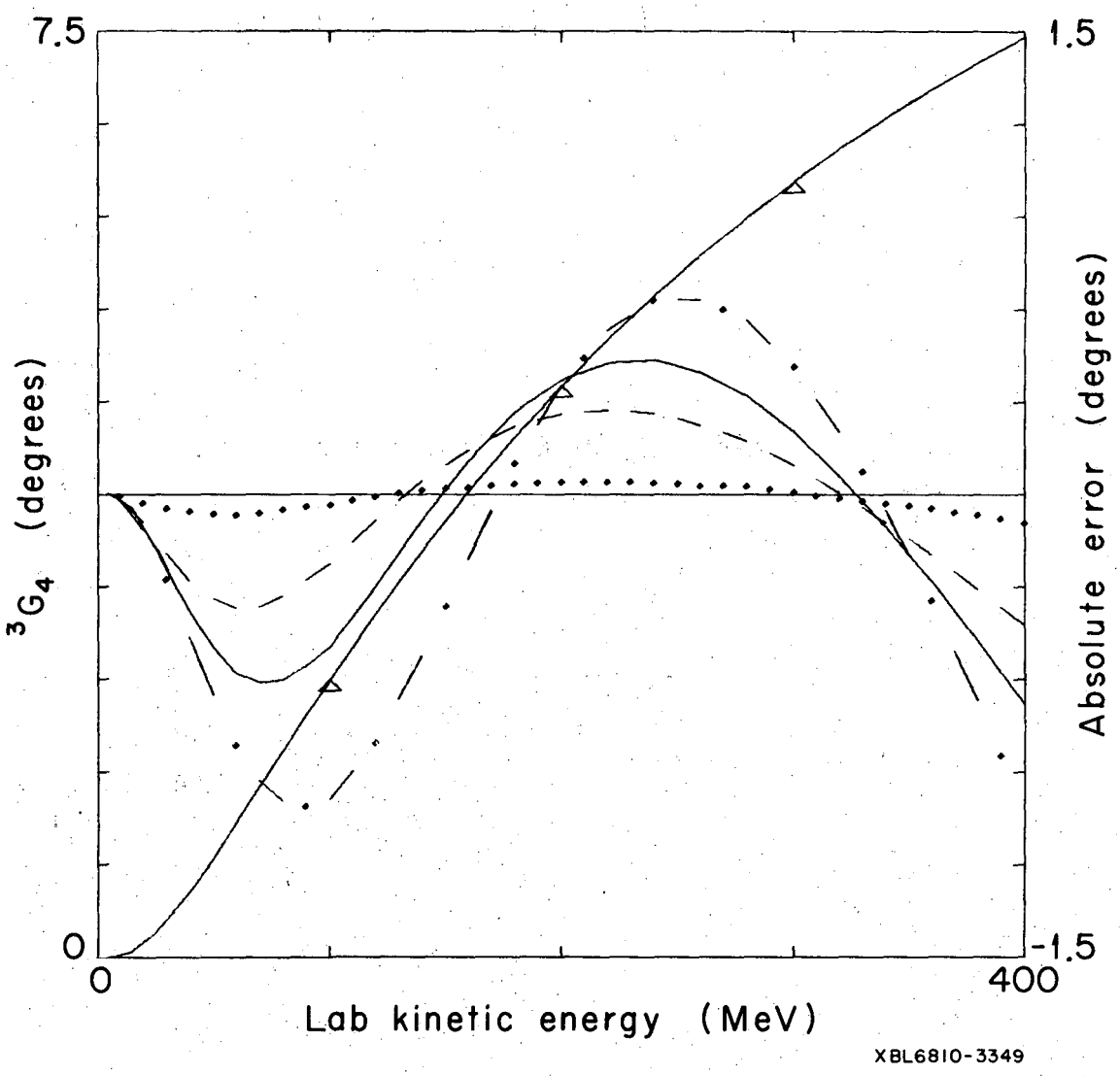
7.5
1.5
$^3G_4$ (degrees)
Absolute error (degrees)
0
-1.5
0
400
Lab kinetic energy (MeV)
XBL6810-3349

Fig. 10

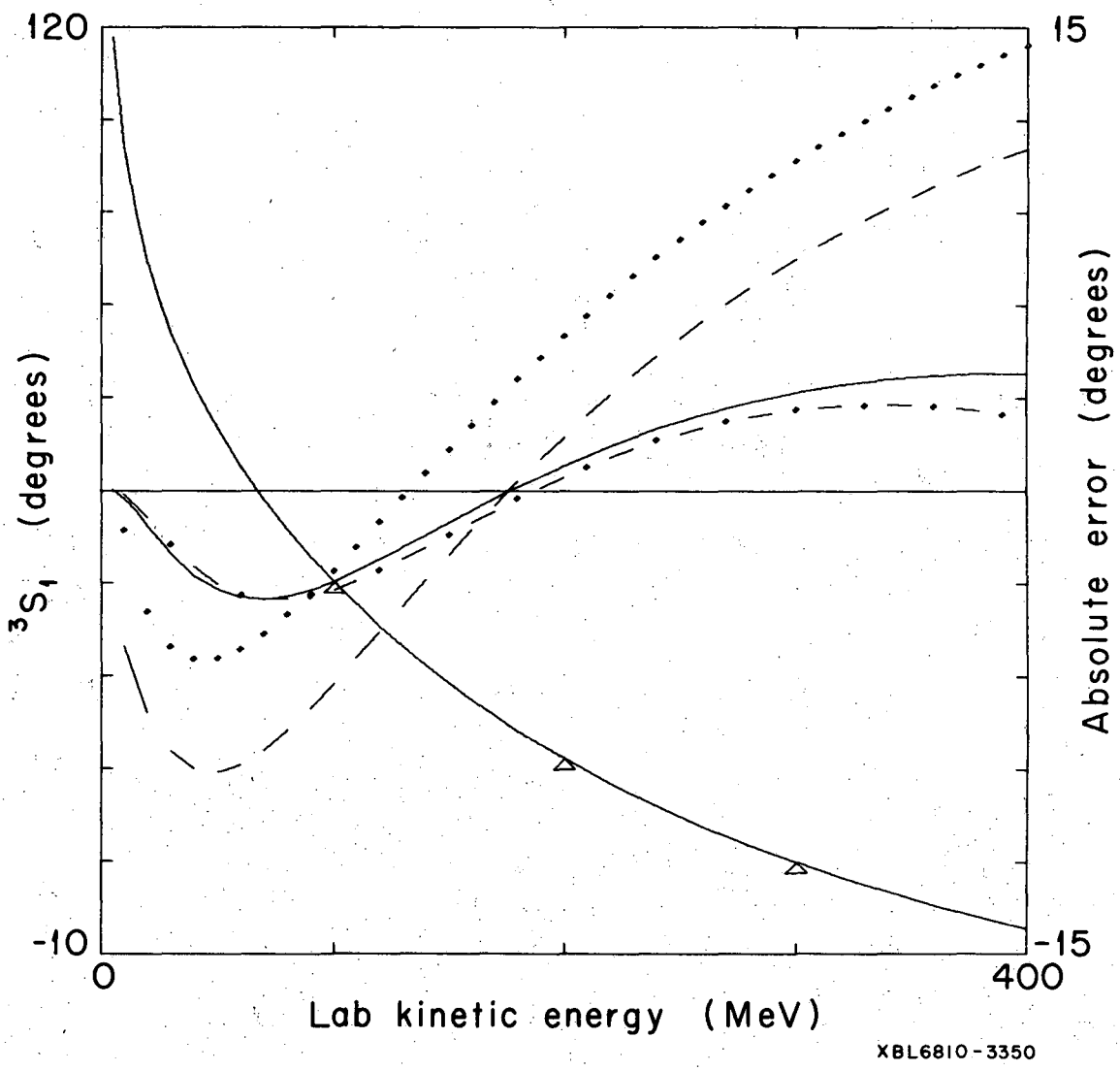
120
-10
0
400
15
-15
$^3S_1$ (degrees)
Absolute error (degrees)
Lab kinetic energy (MeV)
XBL6810-3350

Fig. 11

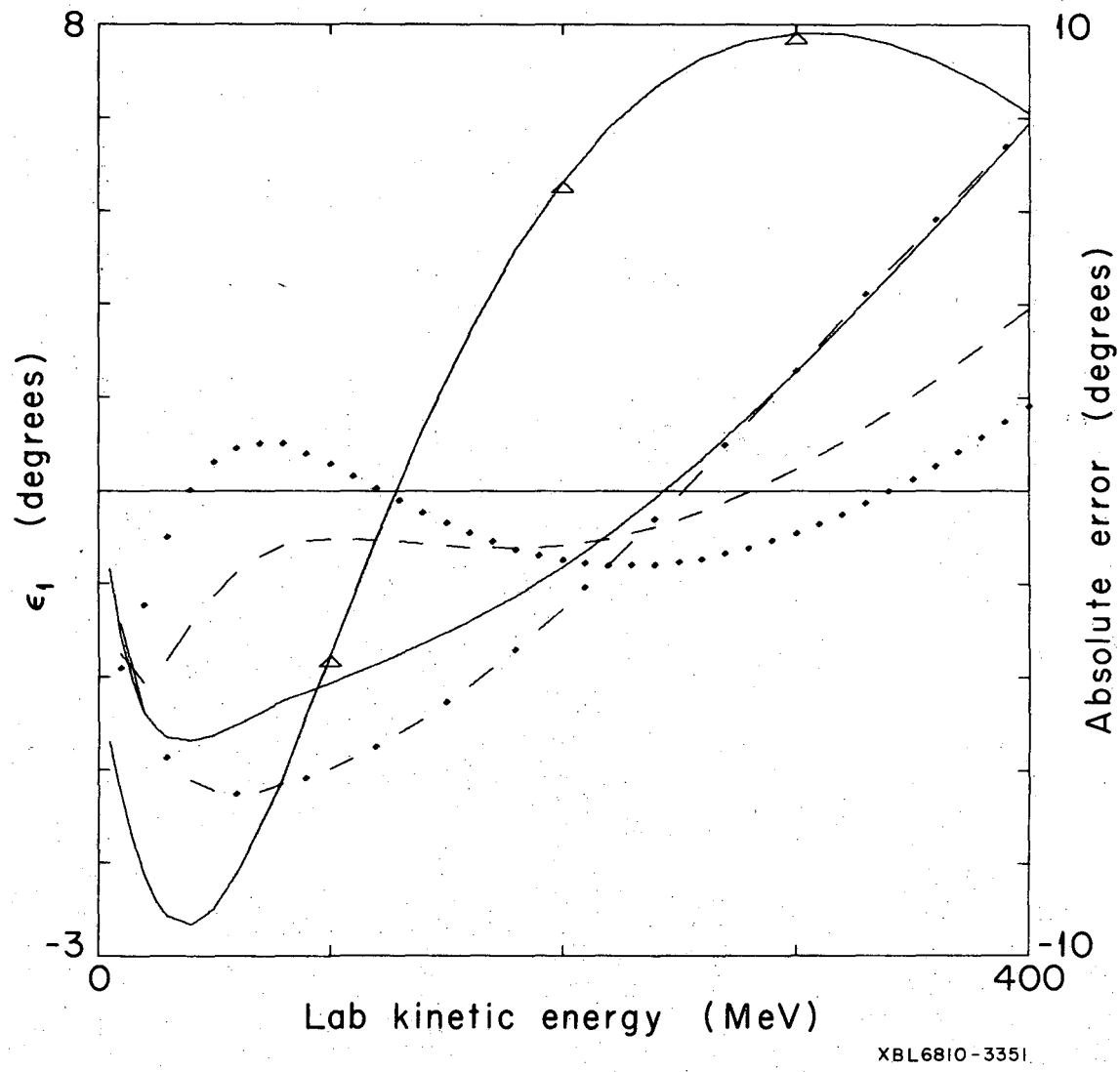
8
10
ϵ_1 (degrees)
Absolute error (degrees)
-3
-10
0
400
Lab kinetic energy (MeV)
XBL6810-3351

Fig. 12

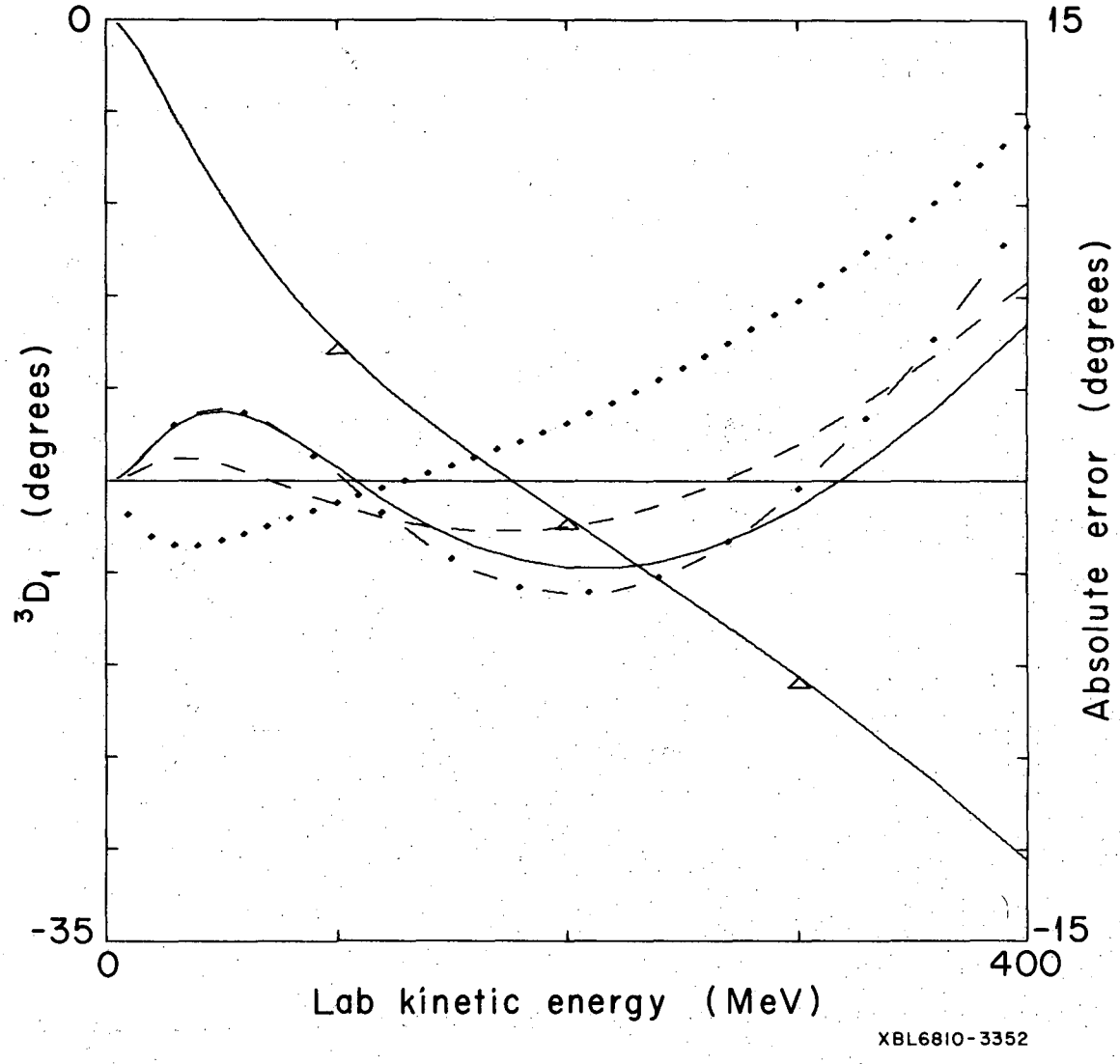
0
15
-35
-15
0
400
$^3D_1$ (degrees)
Absolute error (degrees)
Lab kinetic energy (MeV)
XBL6810-3352

Fig. 13

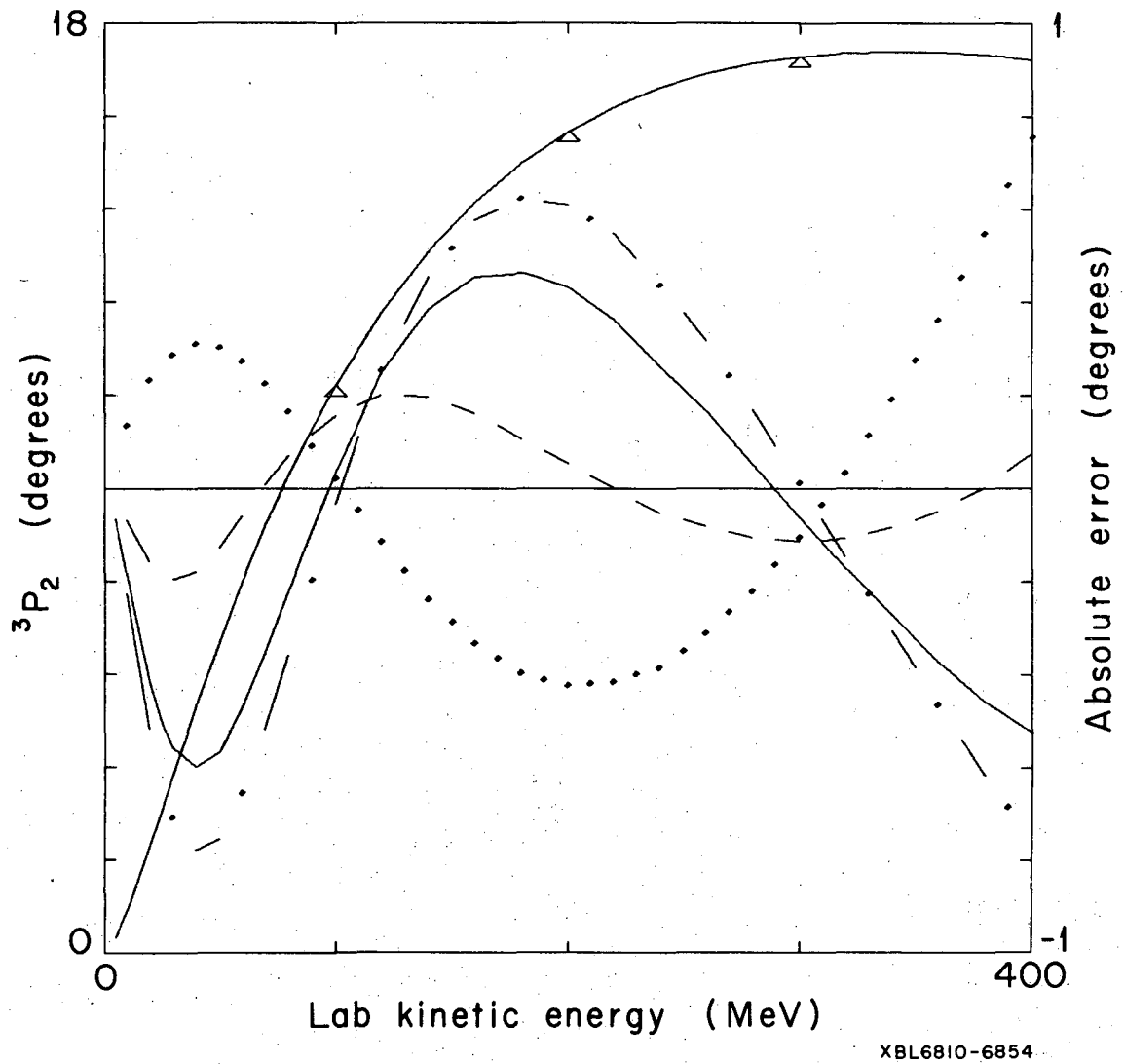
18
1
0
-1
0
400
$^3P_2$ (degrees)
Absolute error (degrees)
Lab kinetic energy (MeV)
XBL6810-6854

Fig. 14

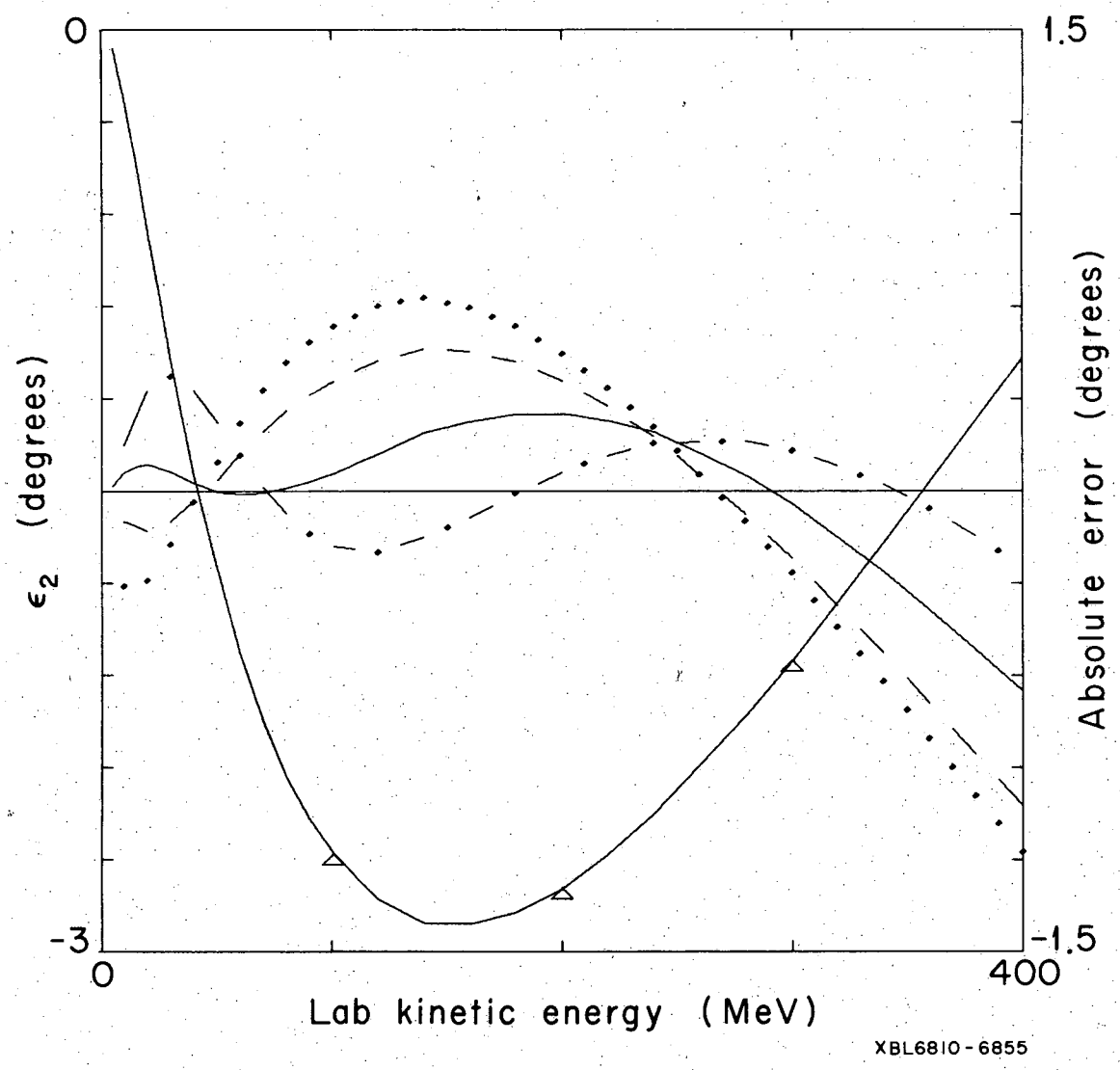
0
1.5
ϵ_2 (degrees)
Absolute error (degrees)
-3
-1.5
0
400
Lab kinetic energy (MeV)
XBL6810-6855

Fig. 15

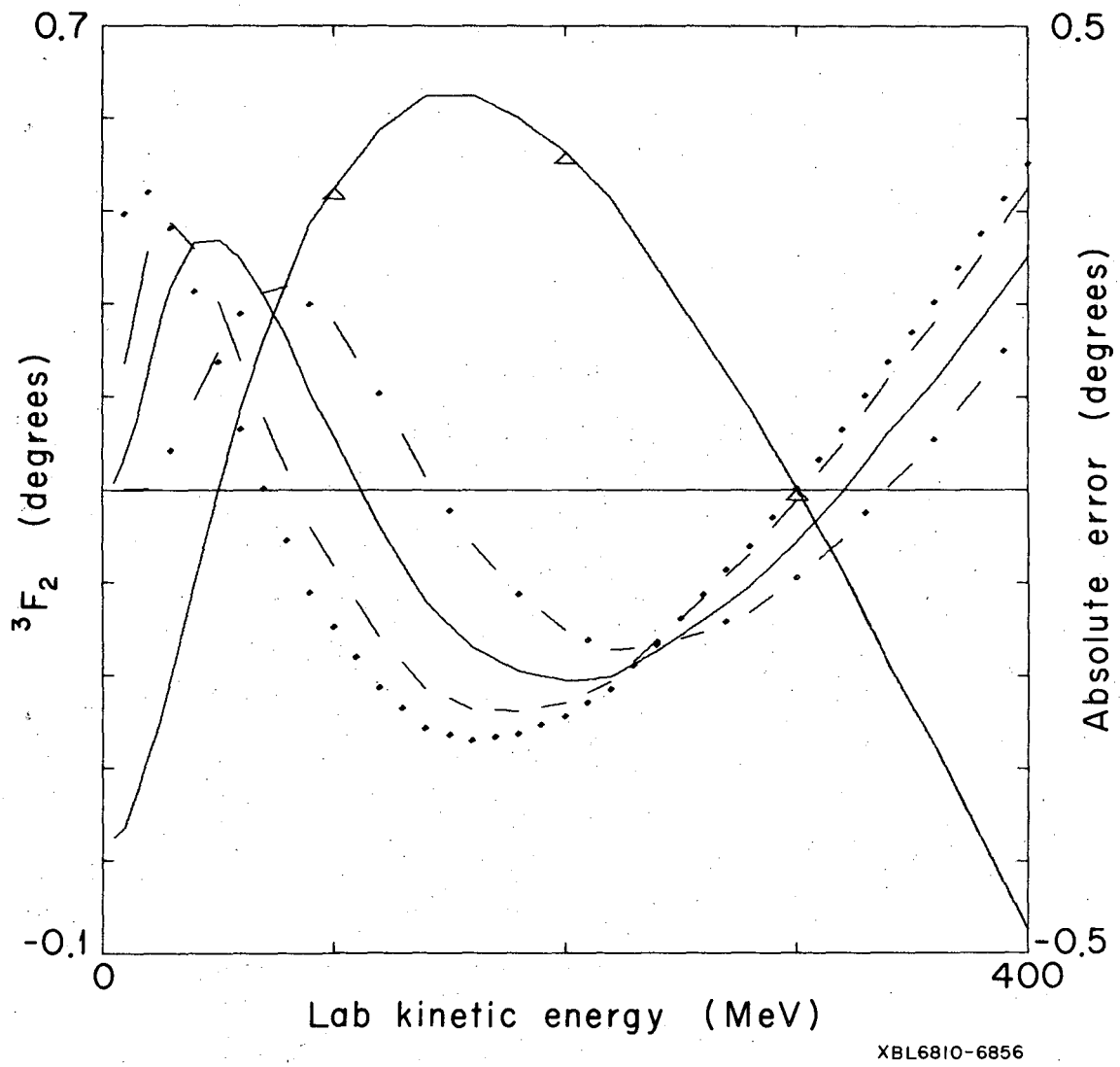
0.7
0.5
$^3F_2$ (degrees)
Absolute error (degrees)
-0.1
-0.5
0
400
Lab kinetic energy (MeV)
XBL6810-6856

Fig. 16

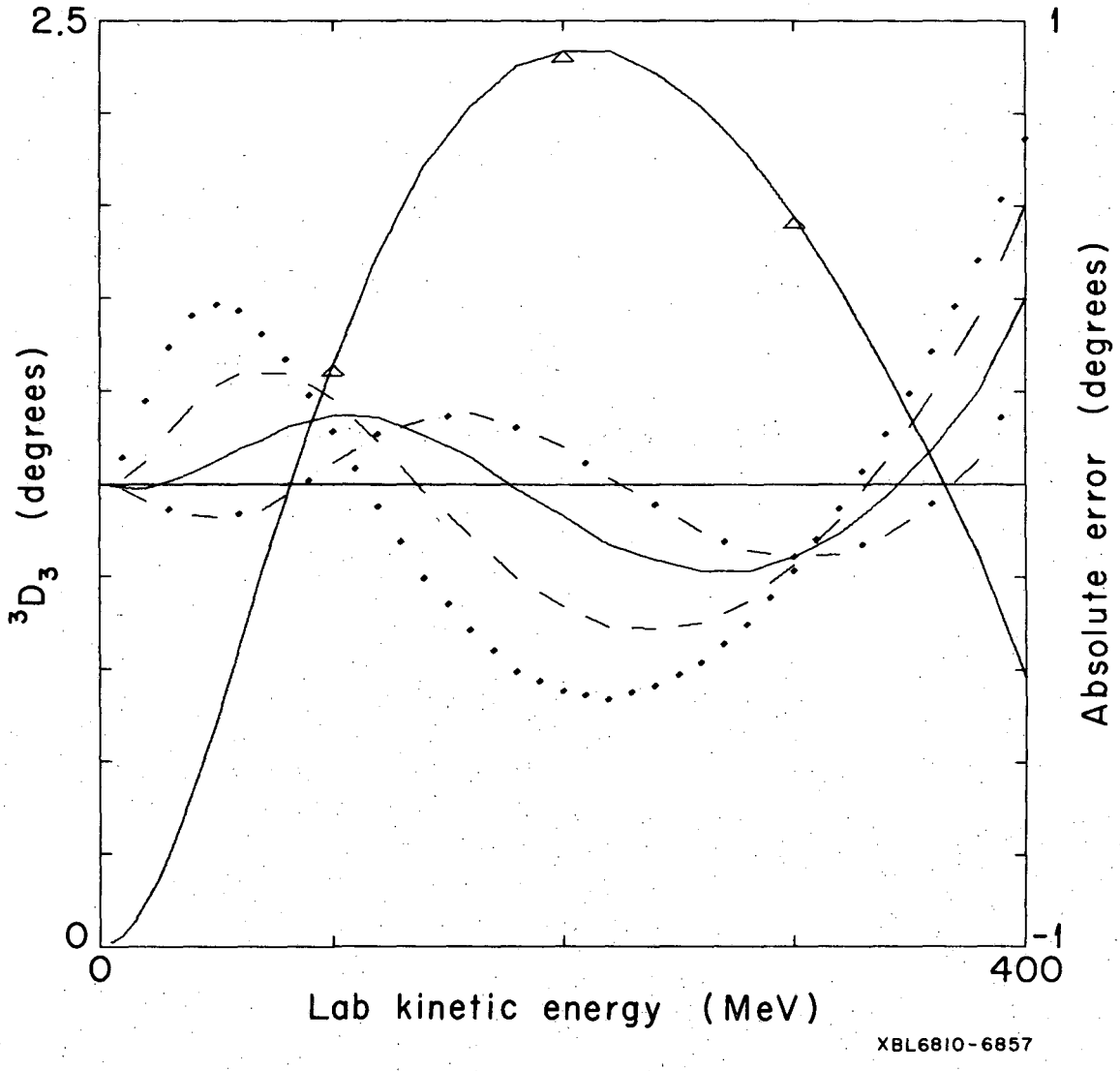
2.5
1
$^3D_3$ (degrees)
Absolute error (degrees)
0
-1
0
400
Lab kinetic energy (MeV)
XBL6810-6857

Fig. 17

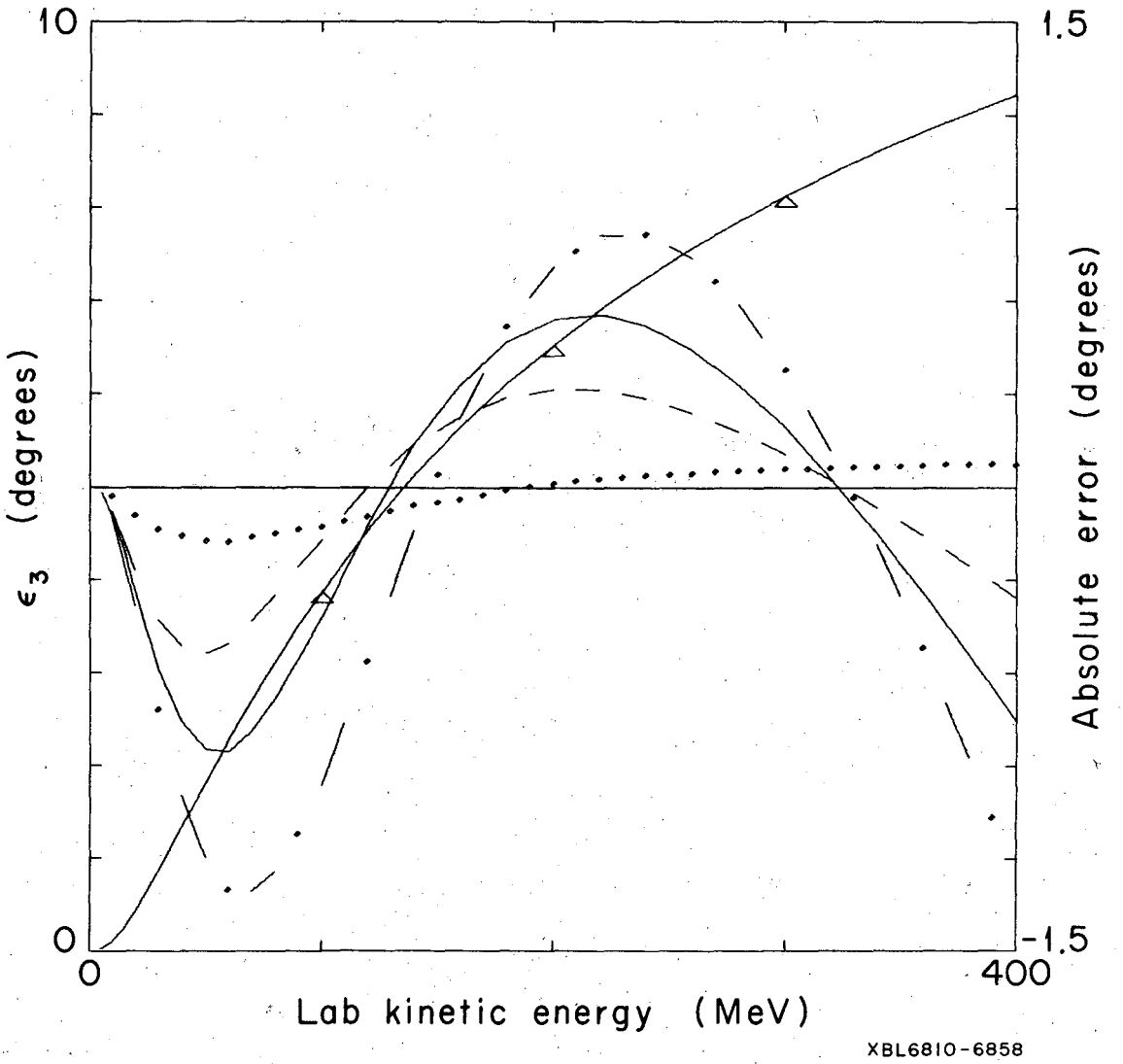
10
0
1.5
-1.5
0
400
ϵ_3 (degrees)
Absolute error (degrees)
Lab kinetic energy (MeV)
XBL6810-6858

Fig. 18

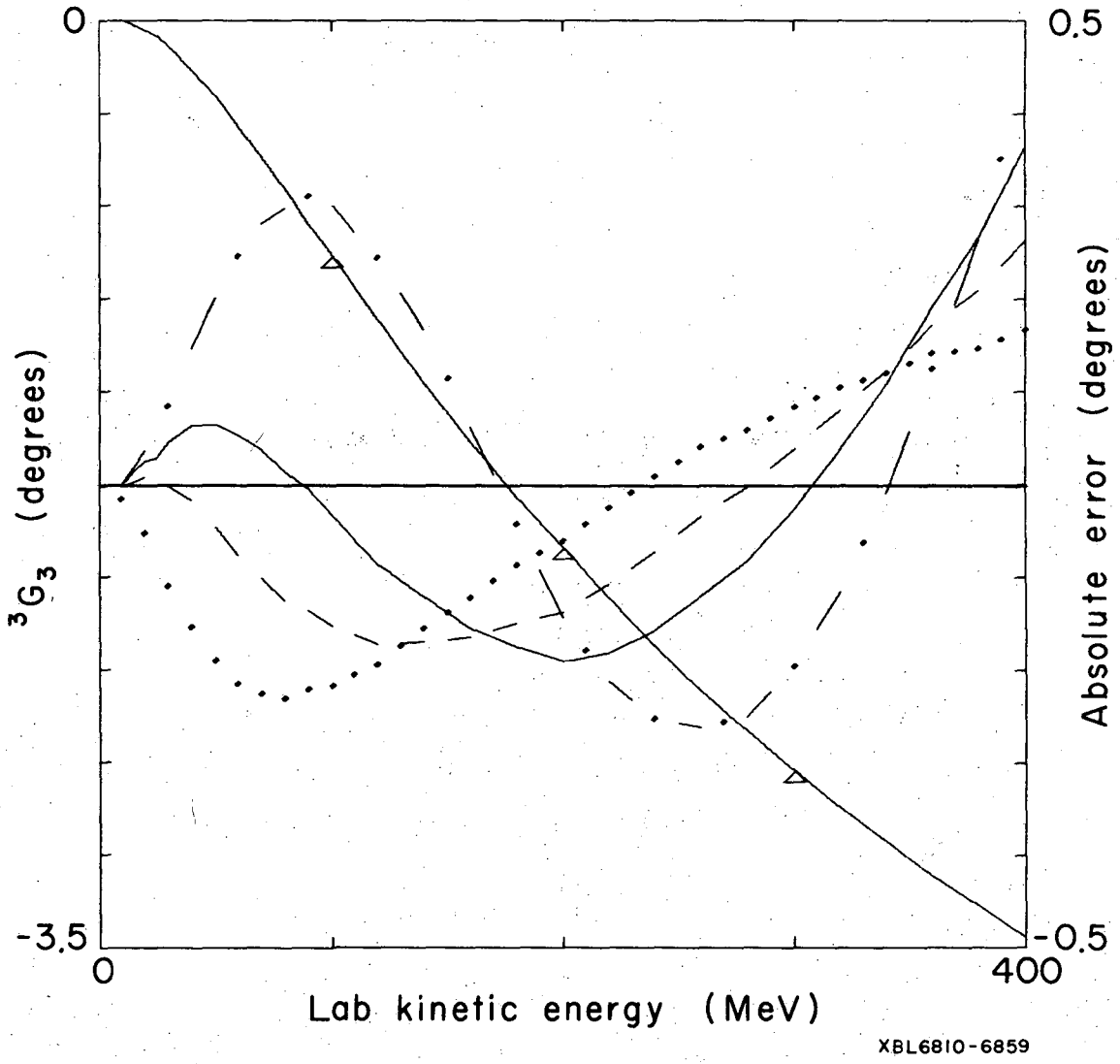
0
0.5
$^3G_3$ (degrees)
Absolute error (degrees)
-3.5
-0.5
0
400
Lab kinetic energy (MeV)
XBL6810-6859

Fig. 19

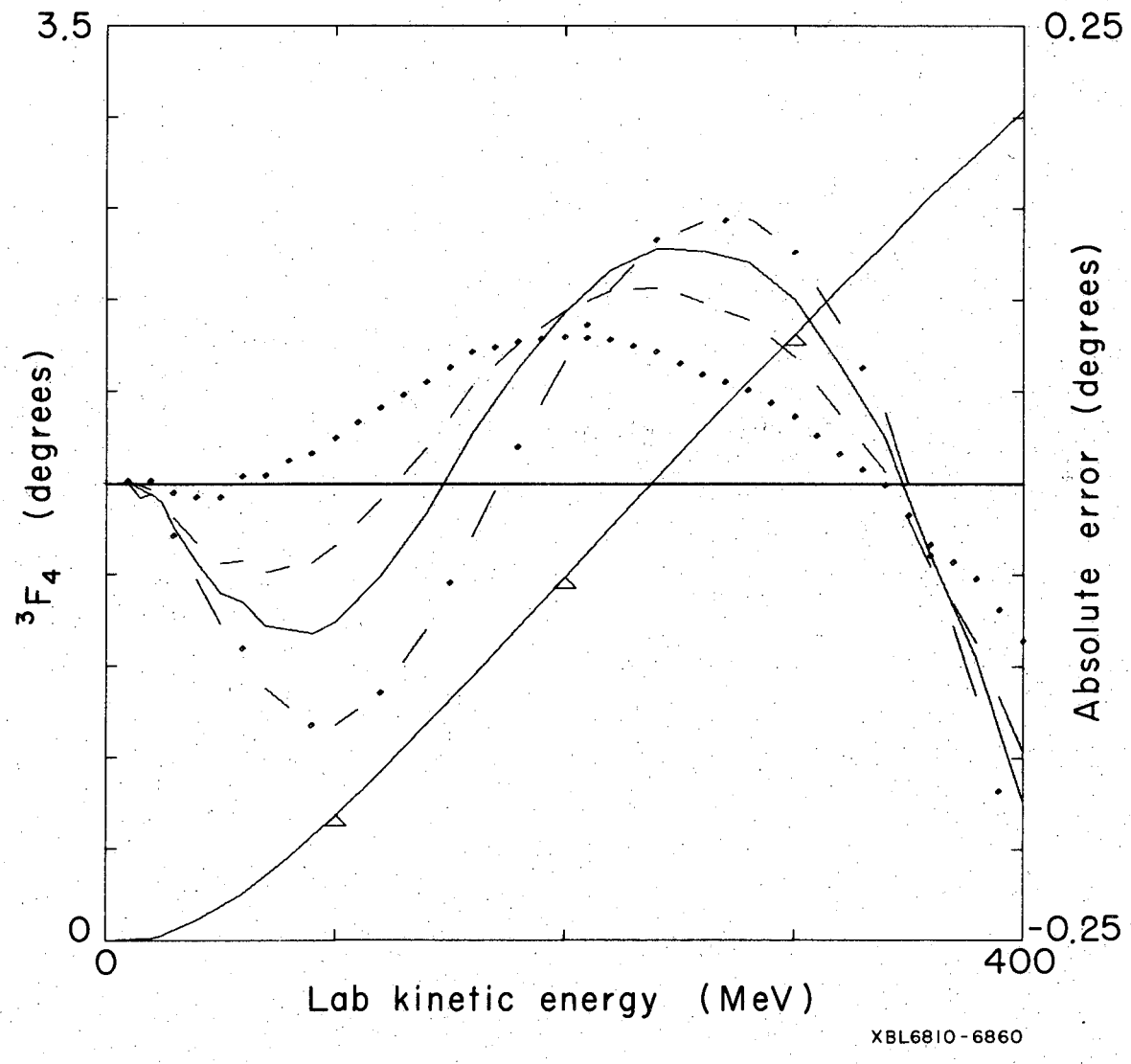
3.5
0.25
$^3F_4$ (degrees)
Absolute error (degrees)
0
-0.25
0
400
Lab kinetic energy (MeV)
XBL6810-6860

Fig. 20

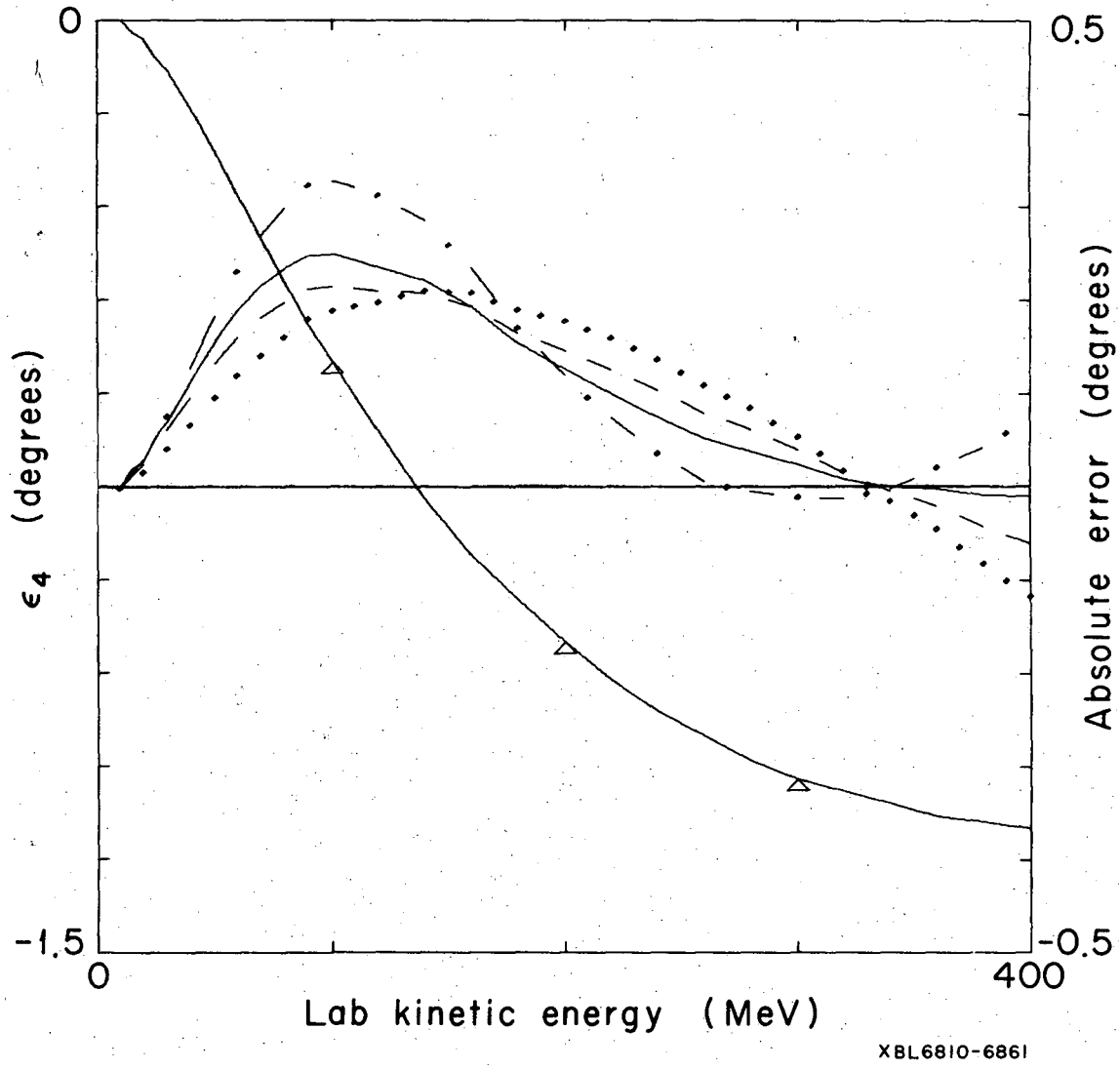
0
0.5
ϵ_4 (degrees)
Absolute error (degrees)
-1.5
-0.5
0
400
Lab kinetic energy (MeV)
XBL6810-6861

Fig. 21

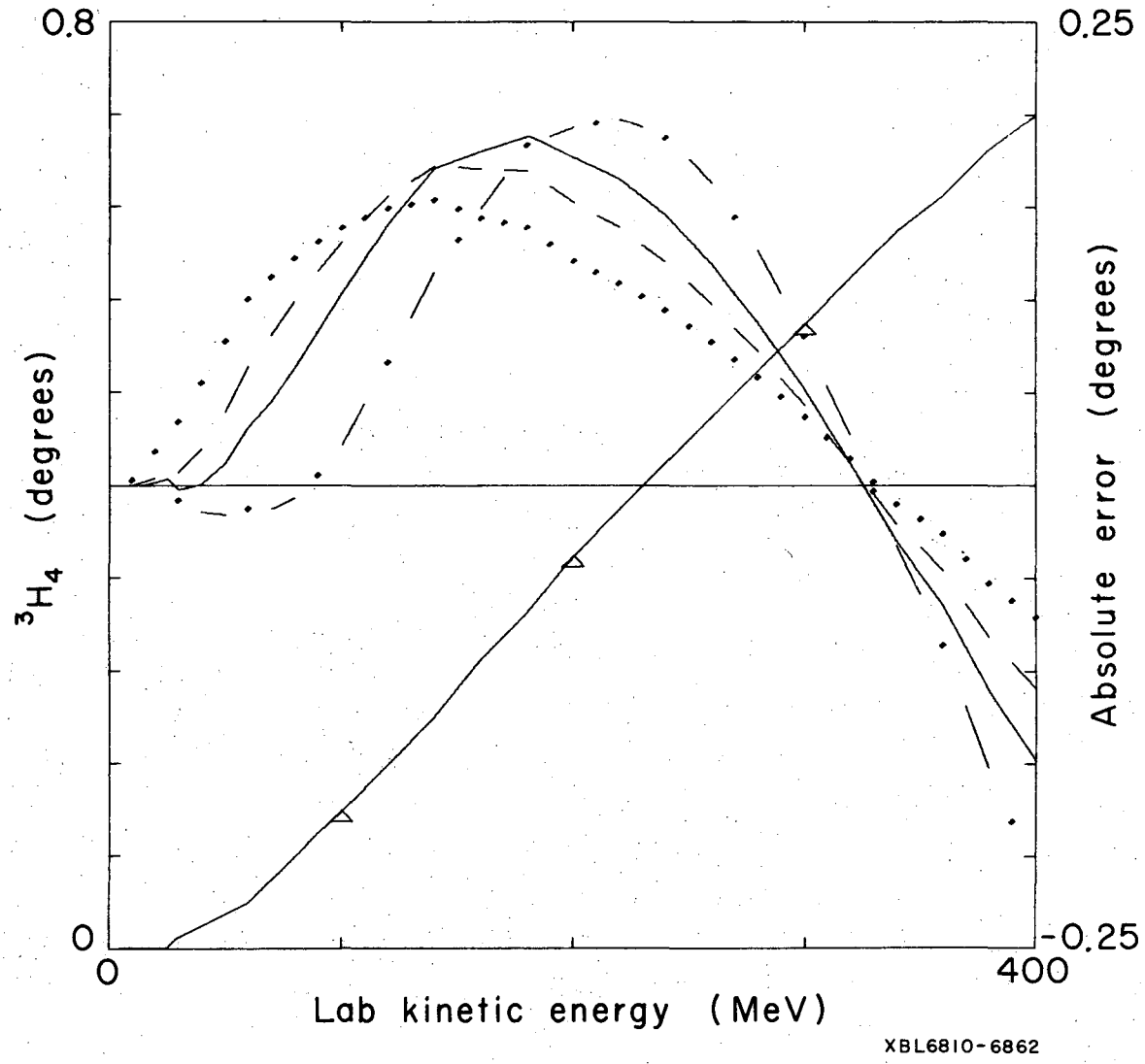
0.8
0.25
$^3H_4$ (degrees)
Absolute error (degrees)
0
-0.25
0
400
Lab kinetic energy (MeV)
XBL6810-6862

Fig. 22

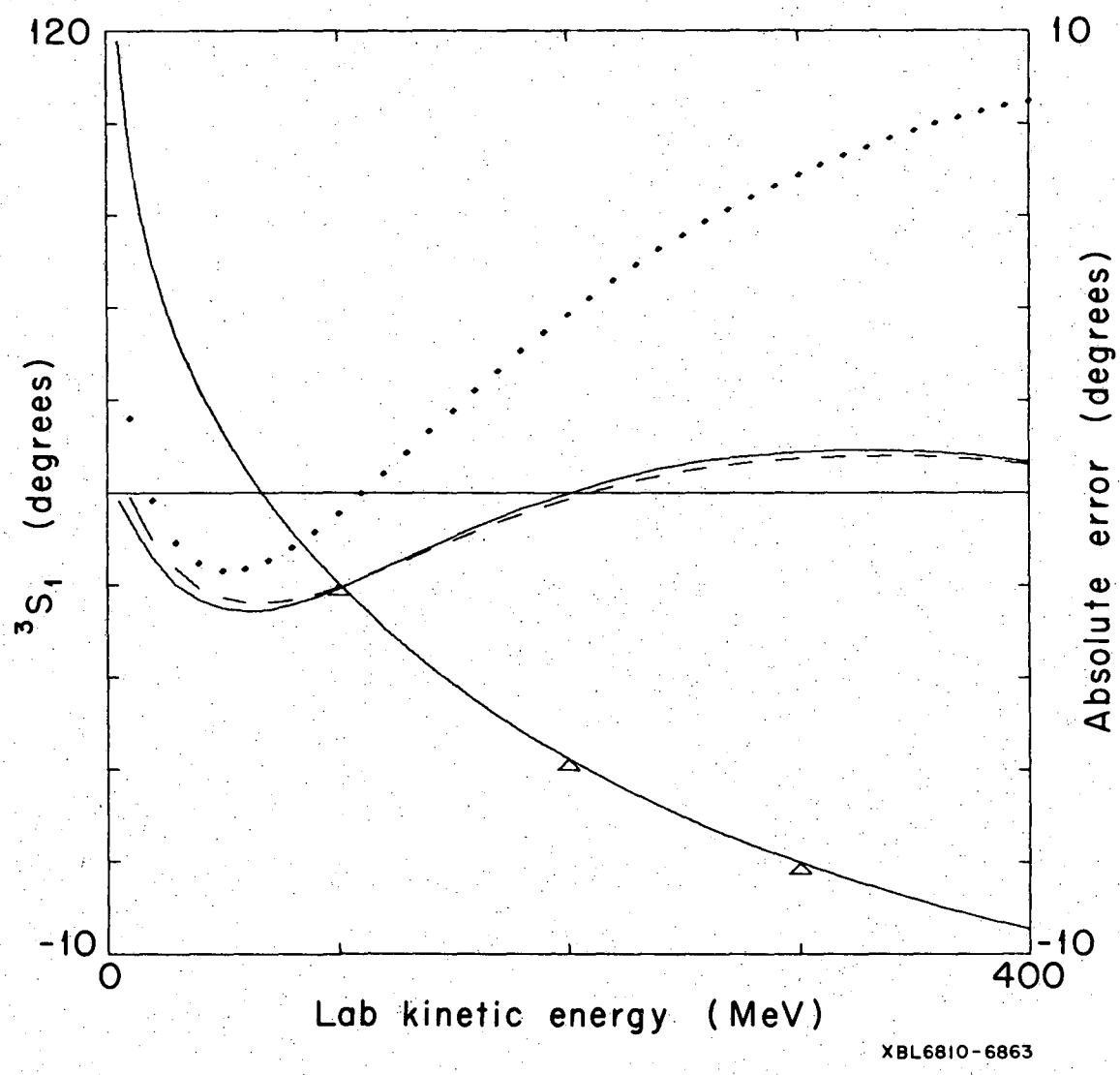
120
10
$^3S_1$ (degrees)
Absolute error (degrees)
-10
-10
0
400
Lab kinetic energy (MeV)
XBL6810-6863

Fig. 23

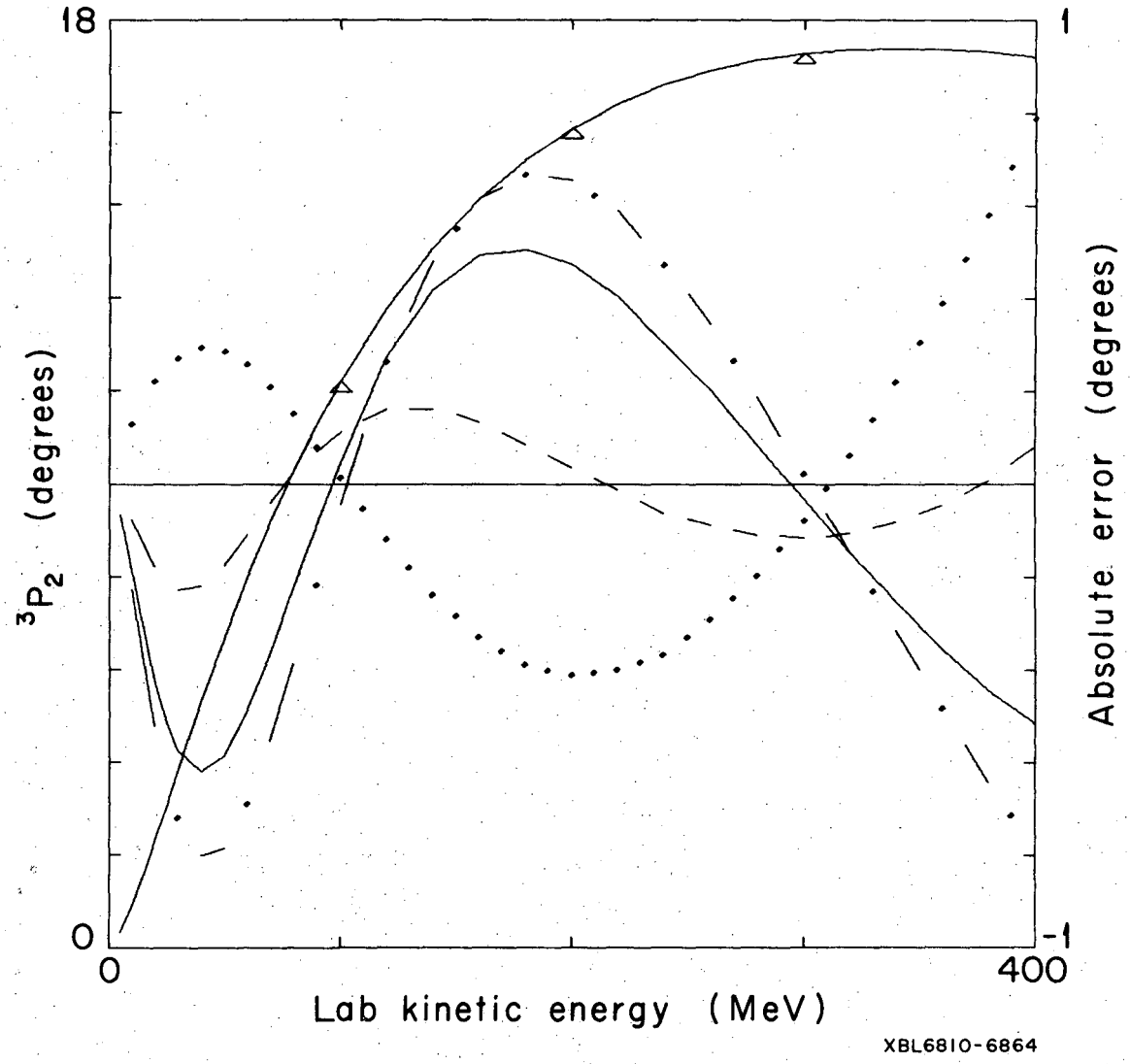
18
1
0
-1
0
400
$^3P_2$ (degrees)
Absolute error (degrees)
Lab kinetic energy (MeV)
XBL6810-6864

Fig. 24

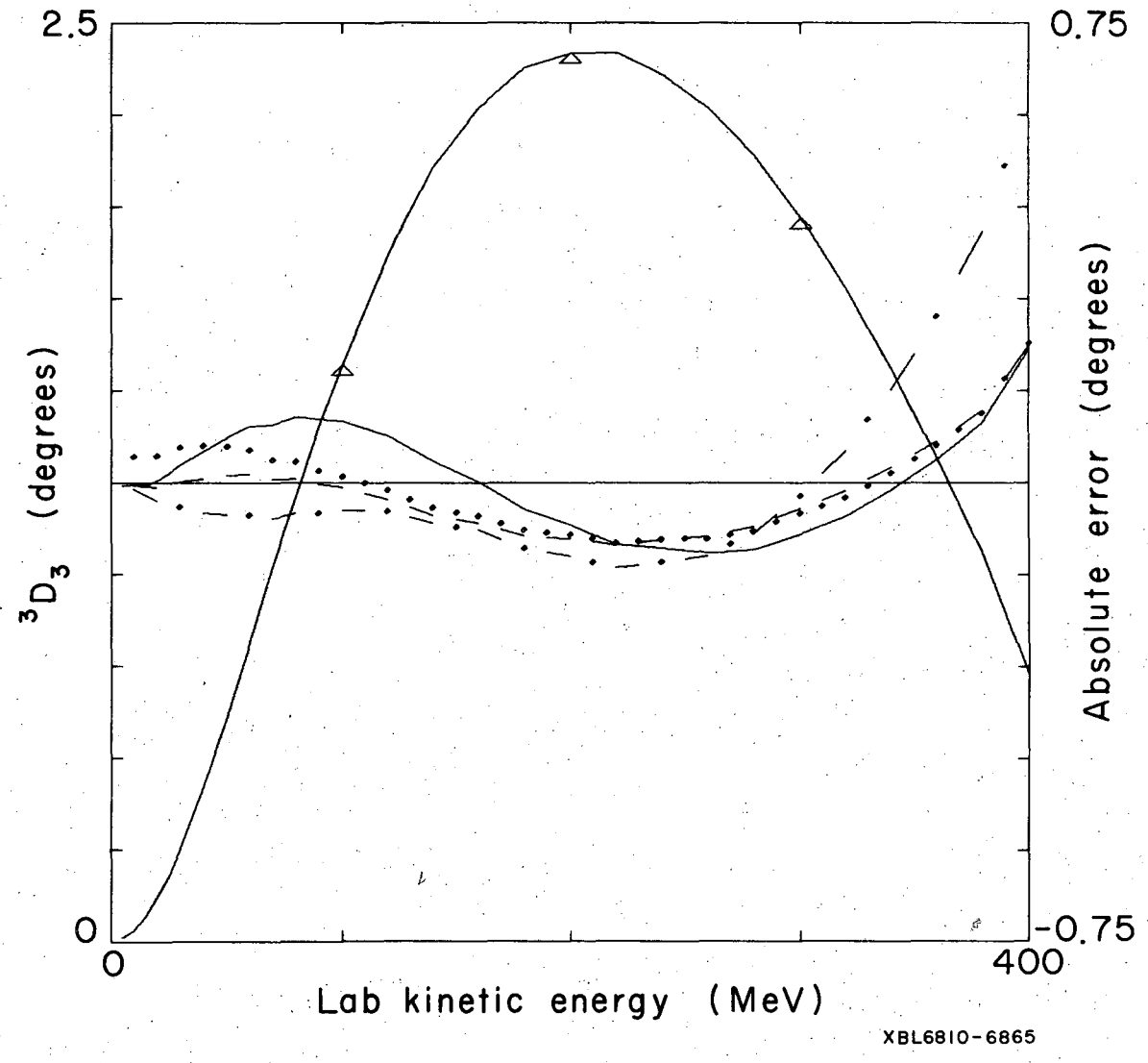
2.5
0.75
$^3D_3$ (degrees)
Absolute error (degrees)
0
-0.75
0
400
Lab kinetic energy (MeV)
XBL6810-6865

Fig. 25

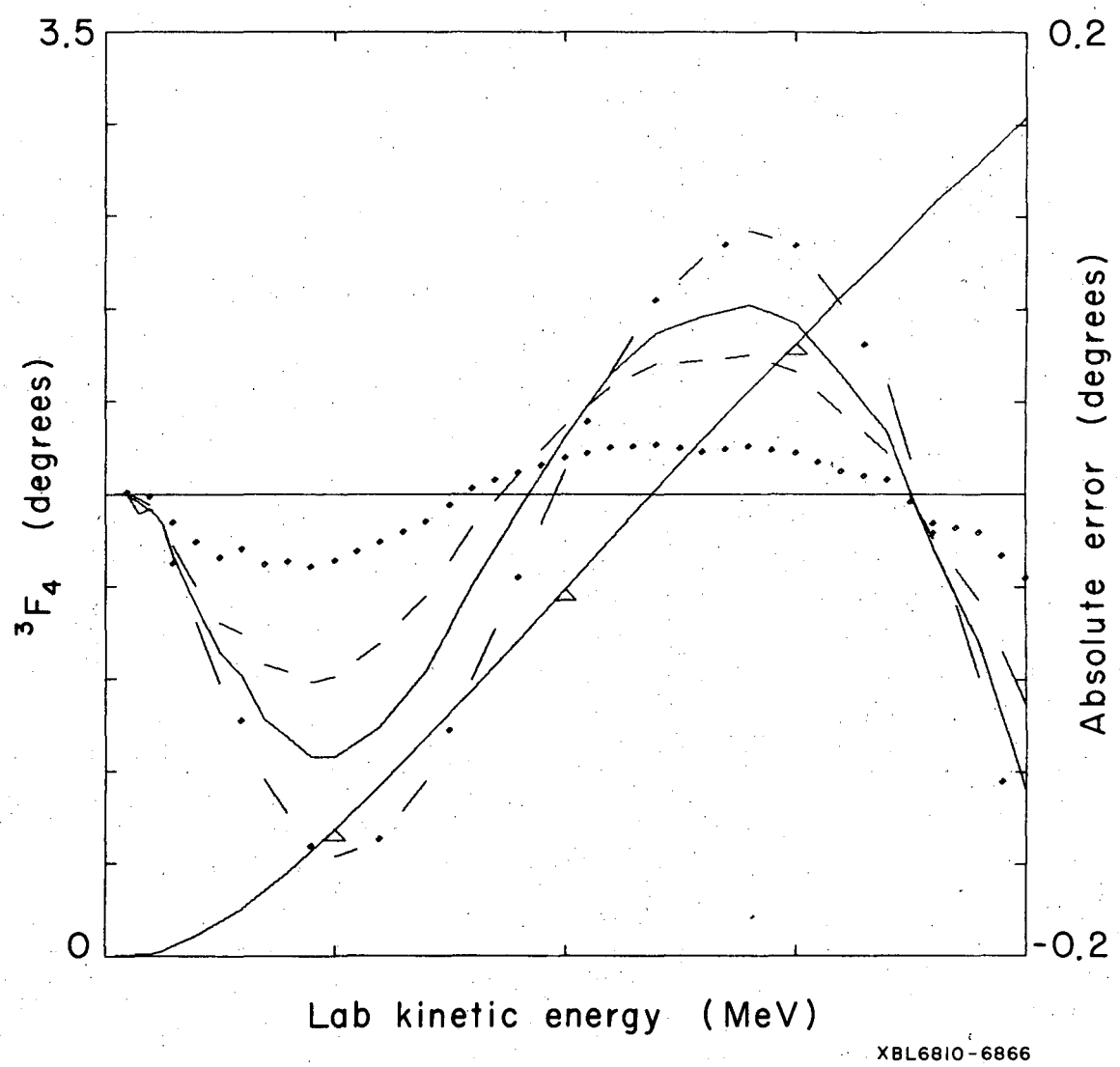
3.5
0
0.2
-0.2
$^3F_4$ (degrees)
Absolute error (degrees)
Lab kinetic energy (MeV)
XBL6810-6866

Fig. 26